

Master's Thesis
석사 학위논문

Metal-Insulator-Metal Diodes for High Frequency
Applications

Jeong Hee Shin(신 정 희 申 定 熙)

Department of Information and Communication Engineering
정보통신융합공학 전공

DGIST

2013

Master's Thesis
석사 학위논문

Metal-Insulator-Metal Diodes for High Frequency
Applications

Jeong Hee Shin(신 정 희 申 定 熙)

Department of Information and Communication Engineering
정보통신융합공학 전공

DGIST

2013

Metal-Insulator-Metal Diodes for High Frequency Applications

Advisor : Professor Jae Eun Jang

Co-advisor : Professor YounGu Lee

by

Jeonghee Hee Shin


Department of Information and Communication Engineering

DGIST

A thesis submitted to the faculty of DGIST in partial fulfillment of the requirements for the degree of Master of Science in the Department of Information and Communication Engineering. The study was conducted in accordance with Code of Research Ethics¹

12. 4. 2012

Approved by

Professor Jae Eun Jang ()
(Advisor)

Professor YounGu Lee ()
(Co-Advisor)

¹ Declaration of Ethical Conduct in Research: I, as a graduate student of DGIST, hereby declare that I have not committed any acts that may damage the credibility of my research. These include, but are not limited to: falsification, thesis written by someone else, and distortion of research findings or plagiarism. I affirm that my thesis contains honest conclusions based on my own careful research under the guidance of my thesis advisor.

Metal-Insulator-Metal Diodes for High Frequency Applications


Jeong Hee Shin

Accepted in partial fulfillment of the requirements for the degree of Master of Science

12. 4. 2012

Head of Committee 장 재 은 

Prof. Jae Eun Jang

Committee Member 이 윤 구 

Prof. YounGu Lee

Committee Member 김 민 수 

Prof. Min-Soo Kim

ABSTRACT

Ultrafast electrical components have been required to apply to various devices such as the high-speed computer, the optoelectronic devices, and the communication systems. Recently for the communication field, the demanded frequency almost approaches THz range [1]. Thus, electrical components, operated in terahertz (THz) area, should be developed. One of the challenging electrical devices is a diode, which has rectifying characteristics. Schottky diode has been used widely to convert alternative current (AC) to direct current (DC) in high frequency area. Unfortunately, the applied frequency of Schottky diodes is limited below THz level [5]. Metal-insulator-metal (MIM) diode has been studied to overcome the frequency limit due to its fast response time. Some MIM diode results have expected theoretically an operation up to 100THz level by the nano-scale small junction dimension and the tunneling current. Therefore, from this structure we can have a motivation to solve the limit for various THz applications.

Our purpose is to improve the asymmetric of I-V curve as well as the decrease of RC (resistance-capacitance) constant time in MIM diode structure for high frequency rectifying performance. To achieve these purposes, a simple vertical MIM diode, a lateral MIM diode, and a metal-insulator-carbon nanotube (MIC) diode have been studied. These devices were fabricated using optical and electron beam lithography, physical vapor deposition (PVD), growth of a vertically aligned carbon nanotube by plasma enhanced chemical vapor deposition (PECVD), and lift-off process. The electric characteristics and figure of merits of these MIM diodes are investigated especially for high-speed operation. The lateral MIM and the MIC structure have shown the nonlinearity and the asymmetric characteristics depending on structural effect and work function difference. Especially in MIC diode, it shows a good rectifying performance up to 10 MHz in direct measurement mode and the estimated maximum cut-off frequency is 3.47 THz.

Keywords: high frequency operation, terahertz (THz), metal-insulator-metal (MIM) diode.

Contents

Abstract.....	i
List of contents	ii
List of tables	iii
List of figures	iv
I. INTRODUCTION	
1.1 Theoretical Background	1
1.1.1 p - n junction & Schottky Diode	1
1.1.2 Tunnel Diode.....	1
1.1.3 MIM tunnel Diode.....	5
1.1.3.1 Characteristics of MIM Diode.....	7
1.1.3.2 Theoretical Model of MIM Diode	9
1.1.3.3 Factors Limiting MIM Diode.....	13
1.1.3.4 Structure Tendency of MIM Diode	13
1.2 Objective.....	15
II. FABRICATTION	
2.1 Fabrication of Simple vertical MIM Diode.....	16
2.2 Fabrication of Lateral MIM Diode	20
2.3 Fabrication of Metal-Insulator-Carbon nanotube (MIC) Diode ...	22
III. ELECTRIC CHARACTERISTICS AND RESULTS	
3.1 Electric Characteristics of Simple vertical MIM Diode	28
3.2 Electric Characteristics of Lateral MIM Diode	33
3.3 Electric Characteristics of MIC Diode.....	41
3.4 Rectification Performance	46
IV. CONCLUSION	50
REFERENCES	52

List of tables

Table 2.1: The description of the samples of simple MIM diodes	17
Table 3.1: Work Functions.....	29
Table 4.1: Comparison with the simple MIM diode, lateral MIM diode, MIC diode	51

List of figures

Figure 1.1: A p - n junction in thermal equilibrium with zero-bias voltage applied	1
Figure 1.2: A schematic and energy band diagram of a Schottky barrier diode	2
Figure 1.3: I-V characteristics of tunnel diode	3
Figure 1.4: Simplified energy band diagrams and current-voltage characteristic of a tunnel diode.....	4
Figure 1.5: The SEM image of a Cat-whisker point contact diode	6
Figure 1.6: Theoretical tunnel resistance as a function of applied voltage for an asymmetrical MIM structure	8
Figure 1.7: An equivalent circuit of MIM diode	9
Figure 1.8: The schematic energy band diagram of MIM diode each bias condition	12
Figure 1.9: The TEM image of the simple MIM diode	14
Figure 1.10: The schematic illustration and SEM image of edge metal-oxide-metal (MOM) diode.....	14
Figure 2.1: The whole process steps of the simple MIM diode	18
Figure 2.2: The simple MIM diode (a) the real pattern design (b) schematic illustration of the simple MIM diode.....	20
Figure 2.3: The whole process steps of the lateral MIM diode.....	21
Figure 2.4: The whole process steps of the MIC diode (3D view).....	25
Figure 2.5: The whole process steps of the MIC diode (Cross-section view)	26
Figure 2.6: The schematic illustration of MIC (metal-insulator-carbon nanotube) structure	27

Figure 3.1: The schematic diagrams and photo image of the a simple MIM diode	28
Figure 3.2: The band diagram of sets of Al-AlO _x -Al, Ni-NiO _x -Ni, Al-AlO _x -Pt	29
Figure 3.3: The TEM image of cross-section view of Al-AlO _x -Al MIM structure	30
Figure 3.4: Electrical characteristics of the MIM structure (a) current densities of various metal contacts (b) fifth-order polynomial fit of graph of various metal contacts	31
Figure 3.5: Electrical characteristics of the MIM structure (a) I-V characteristics of various size of junction area of Al-AlO _x -Pt (b) fifth-order polynomial fit	32
Figure 3.6: The description of the measurement of Al-AlO _x -Probe tip structure on the Si/SiO ₂ substrate with moving to Z-location	34
Figure 3.7: Electrical characteristics of the Al-AlO _x -Probe tip structure (a) the I-V characteristics (b) fifth-order polynomial fit.....	35
Figure 3.8: The description of the measurement of Al-SiO ₂ -Probe tip structure on the Si/SiO ₂ substrate with moving to Z-location	36
Figure 3.9: The I-V curve of the Al-SiO ₂ -Probe tip structure	37
Figure 3.10: SEM image of the lateral MIM structure (a) the lateral structure with narrow gap (b) magnified view of gap of the lateral structure	38
Figure 3.11: The electrical characteristics of lateral MIM diode (a) I-V curve of Nb-SiO ₂ -Pt lateral MIM structure with gap approximately 41 nm (b) the plot based on Fowler-Nordheim tunneling model.....	40
Figure 3.12: The schematic illustration of the MIC diode	41
Figure 3.13: The various simulation results based on the electric potential of the MIC structure using COMSOL	42

Figure 3.14: The photo image and SEM image after forming catalyst on the Nb bottom electrode with thin SiO ₂ layer for the MIC diode.....	43
Figure 3.15: The photo image of the whole MIC structure and SEM image of a vertical aligned multi-walled carbon nanotube (MWCNT) using PECVD with C ₂ H ₂ /NH ₃ gas flow, 600V of plasma intensity, 650 °C of temperature, and 10 minute of growth time on patterned Ni catalyst position	43
Figure 3.16: The electrical characteristics of MIC diode (a) I-V curve of Nb-SiO ₂ -MWCNT structure (b) the plot based on Fowler-Nordhiem tunneling model	44
Figure 3.17: I-V characteristics of MIC structure without a CNT	45
Figure 3.18: the measurement set-up for rectification performance	47
Figure 3.19: Rectification performance of Schottky barrier diode (a) 60 Hz (b) 1 kHz (c) 500 kHz (d) 10 MHz.....	47
Figure 3.20: Rectification performance of simple MIM diode (a) 60 Hz (b) 1 kHz (c) 500 kHz (d) 10 MHz	48
Figure 3.21: Rectification performance of lateral MIM diode (a) 60 Hz (b) 1 kHz (c) 500 kHz (d) 10 MHz	48
Figure 3.22: Rectification performance of MIC diode (a) 60 Hz (b) 1 kHz (c) 500 kHz (d) 10 MHz.....	49

I. INTRODUCTION

1.1 Theoretical Background

1.1.1 p - n junction & Schottky Diode

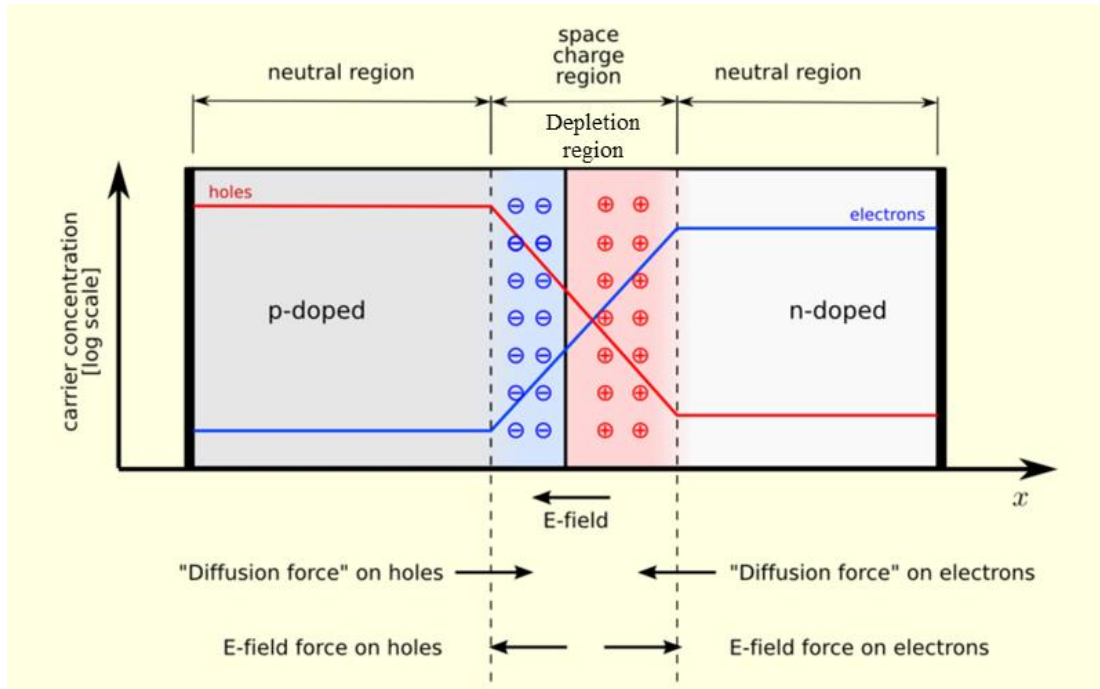


Figure 1.1: A p - n junction in thermal equilibrium with zero-bias voltage applied [1]

The p - n junction is generally used as diodes, a transistor, and solar cells in solid state electronics. When p -type and n -type materials are located in contact with each other, the junction behaves rectification from depletion region, as shown in Figure 1.1. The rectification is to allow an electric current to pass through depletion area in forward direction, while blocking electric current in reverse direction. The p - n junction diode is generally used to convert alternating current (AC) to direct current (DC). However, this mechanism is not suitable for high speed rectification due to the large width of depletion region.

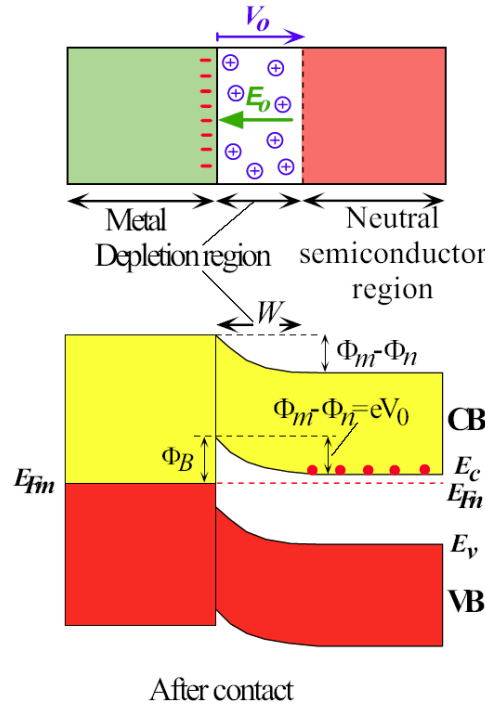


Figure 1.2: A schematic and energy band diagram of a Schottky barrier diode [2]

The Schottky barrier diode (SBD) is one of the high-speed diodes composed of metal-semiconductor junction. Compared to p - n junction, Schottky barrier has much faster mechanism due to narrower junction region and major carrier movement so that it is one of the promising techniques for increasing operating frequency. Also its asymmetric I-V characteristic is enough to commercialize SBD to market for various applications. The most important advantages of Schottky barrier are a lower forward voltage operation and lower noise generation for applications. However, the estimated driving frequency limit is less than 5 THz [3, 4]. For much higher frequency applications, the new system or design is required.

1.1.2 Tunnel Diode

The tunnel diode is a type of semiconductor diode which is available to be very fast operation by using the quantum mechanical effect. It was invented by Leo Esaki when he was studying heavily doped germanium p - n junctions [5]. By quantum mechanical tunneling, an

anomalous current-voltage characteristic in the forward direction and a negative-resistance region were observed in heavily doped diodes. The level of doping of normal p - n junction diode is very low, composing wide depletion region. In the normal p - n junction, tunneling effect cannot be observed. Only when the applied voltage is enough to surmount the potential barrier of the junction, conduction takes place in the normal p - n junction diode. In tunnel diode, heavily doped semiconductor materials (typically $> 10^{19}/\text{cm}^3$) are used to form a junction. An extremely narrow depletion region can be produced by heavy doping. Also heavy doping induces the anomalous current-voltage characteristic with a negative-resistance region compared to that of a normal junction diode.

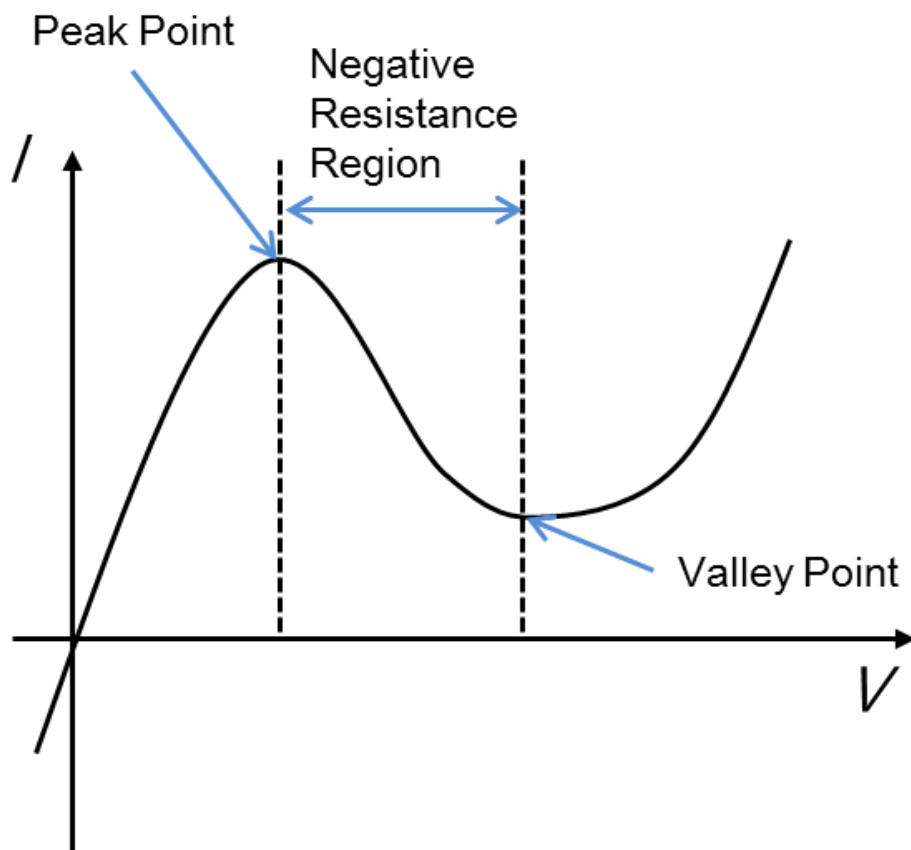


Figure 1.3: I-V characteristics of the tunnel diode [6]

Figure 1.3 shows I-V characteristics of tunnel diode focused on forward direction. Referred to current axis, the tunneling takes place between origin point and valley point. The tunneling current increases up to the valley point. After valley point, referred to voltage axis, the current flow is occurred by overcoming a barrier. The tunneling device can be operated with lower threshold voltage than general surmount mechanism so that this mechanism is able to be widely used for high-speed devices.

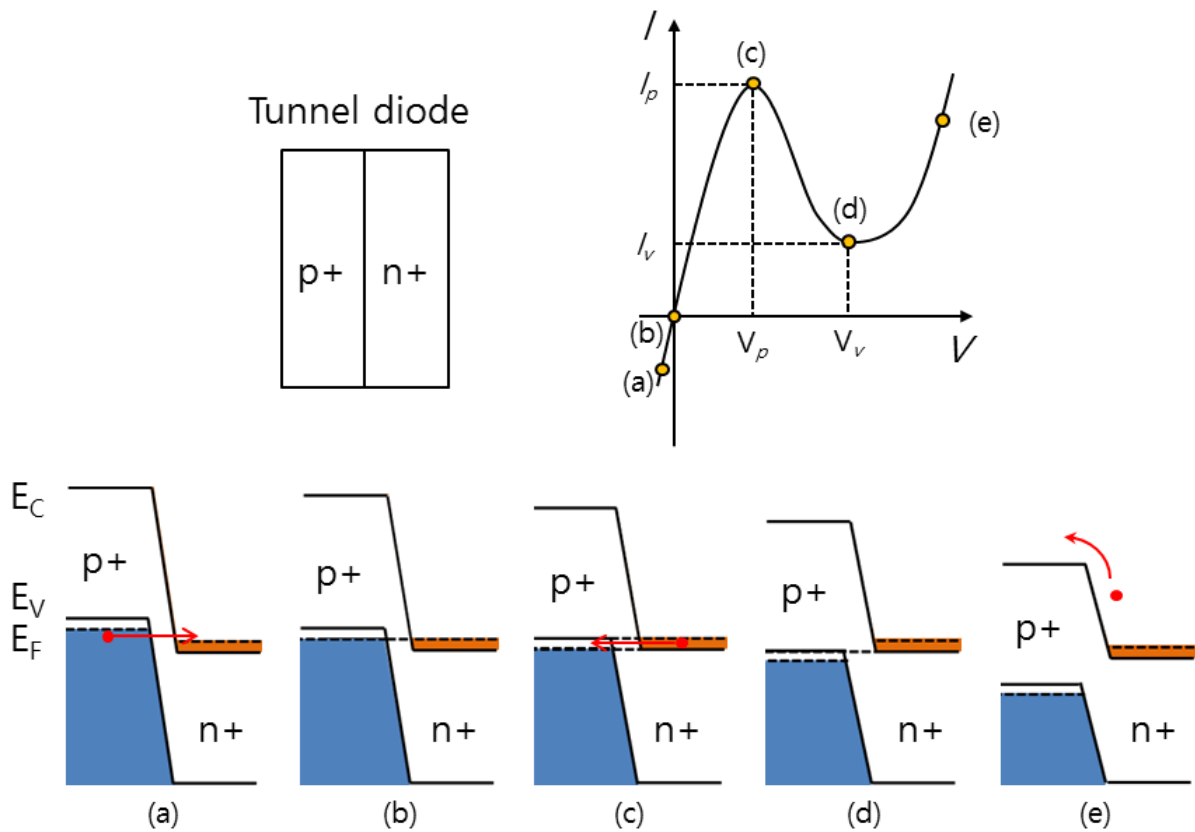


Figure 1.4: Simplified energy band diagrams and current-voltage characteristic of a tunnel diode

The necessary conditions for tunneling are: (1) occupied energy states exist on the side from which the electron tunnels; (2) unoccupied energy states exist at the same energy level on the side to which the electron can tunnel; (3) the tunneling potential barrier height is low and the barrier width is small enough that there is a finite tunneling probability; and (4) the momentum is conserved in the tunneling process [7]. Figure 1.4 shows I-V characteristics and simplified energy band diagrams of a tunnel diode to describe conduction mechanism at (a) reverse bias with increasing tunneling current; (b) thermal equilibrium; (c) forward bias V such that peak current is obtained; (d) forward bias approaching valley current; and (e) forward bias with diffusion current and no tunneling current [7]. When reverse bias is applied to tunnel diode as (a), the valence band is closed to conduction band so that the electrons in valence band can move to conduction band. In thermal equilibrium, there is no electron movement. From origin to V_v , the electron tunnel from conduction band to valence band. After V_v point, referred to voltage axis, conduction mechanism is surmounting a potential barrier. This mechanism is the fastest movement of electrons than others; thus, it is suitable for high-speed rectification.

1.1.3 MIM Tunnel Diode

Metal-insulator-metal (MIM) tunnel diode is capable of high-speed rectification, employing the quantum mechanical effect. This structure is composed by two metals and very thin insulator layer for tunneling effect which leads the lowest threshold voltage. It indicates that the tunneling takes place at lower operating voltage than p - n junction and Schottky barrier so that the MIM tunnel diode is more suitable for high-speed operation; thus, it can be used for infrared and optical radiation detectors as mixer [7].

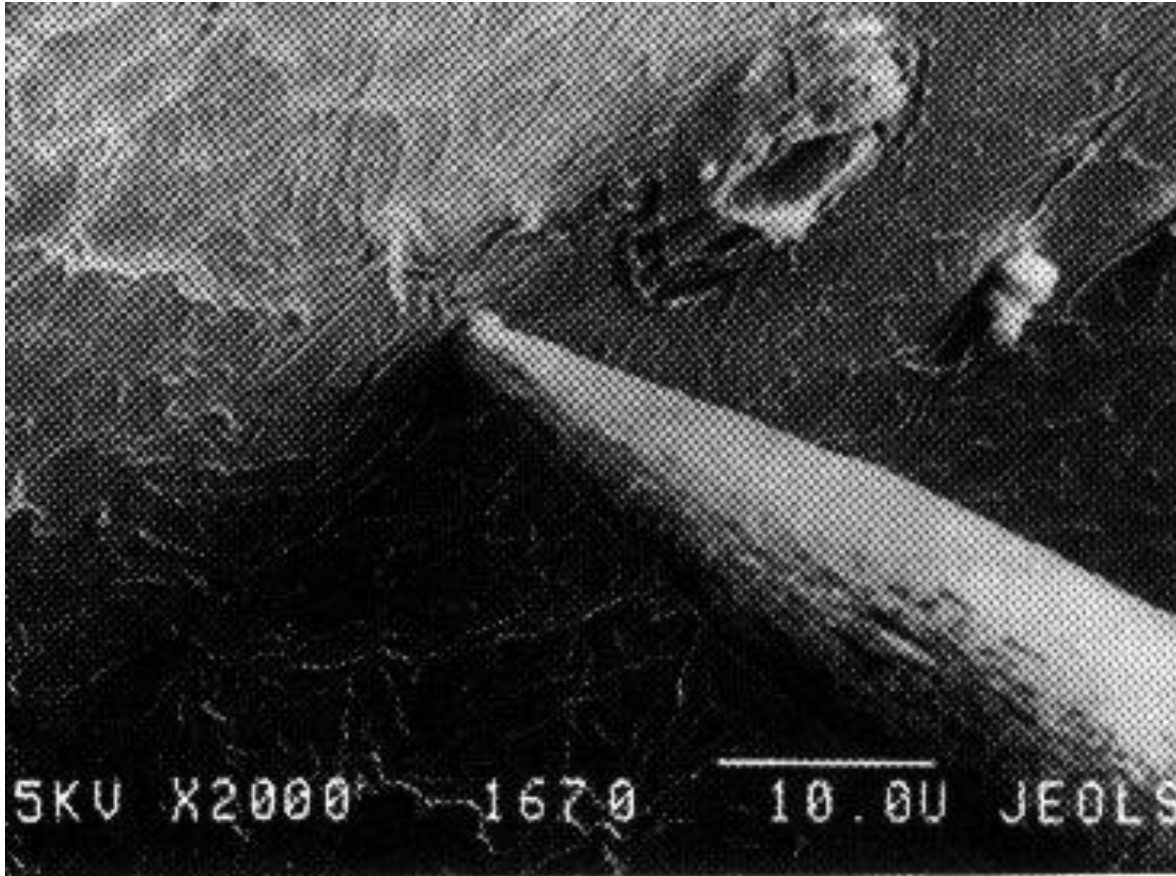


Figure 1.5: The SEM image of a Cat-whisker point contact diode [10]

The earliest MIM device reported in the literature utilized a cat whisker tungsten wire in contact with a polished metal plate for detection of THz waves, as shown in Figure 1.5. The contact was not ohmic, and it was assumed that the conduction is induced by means of electrons tunneling through this uncontrolled insulator. This particular configuration causes very small capacitance and a low resistance, which leads to a short RC constant time [8]. In spite of mechanically instable issue, the point contact configuration has been expected to use in communication field for high-speed rectification from few gigahertz to 150 THz [3, 9].

1.1.3.1 Characteristics of MIM Diode

To become an ideal MIM diode it needs two requirements, the asymmetric I-V characteristics and the short response time. The asymmetric I-V characteristics are relevant to conversion efficiency for rectifying performance. The I-V characteristics of perfect rectification are required to maximize the conversion efficiency. The shorter response time induces a high-speed rectification. This requirement makes its operation range increase over infrared and optical region so that it can get opportunity for various applications. These two requirements are very important to make better performance and to increase the operating frequency.

To make asymmetric I-V characteristics in the MIM diode, the metal electrodes have to be dissimilar with large work function difference. Figure 1.6 shows the tunnel resistance in the asymmetrical MIM structure, applied to either the metal or another metal with various thickness of insulator layer, $d = 20, 30$ and 40 \AA , $\Phi_1 = 1 \text{ V}$, $\Phi_2 = 2 \text{ V}$. The asymmetric structure can make different tunnel resistance, when applying voltage to metal 1 or metal 2, continuous line and discrete line from each thickness, as shown in Figure 1.6. This shows that dissimilar material can make current flow be different depending on the polarity of voltage. Figure 1.6 also indicates that the tunnel resistances for different polarities are different. For an ideal asymmetrical MIM structure in the low voltage range $0 < V < \Phi_1$, the quantities $\Delta d = d$ and $(\Phi_1 + \Phi_2 - V)/2$ (average barrier) are independent of the polarities. Thus the I-V characteristics are also independent of the polarity. At higher voltage, $V > \Phi_2$, the average barrier height and the effective tunneling distance Δd become polarity-dependent [7].

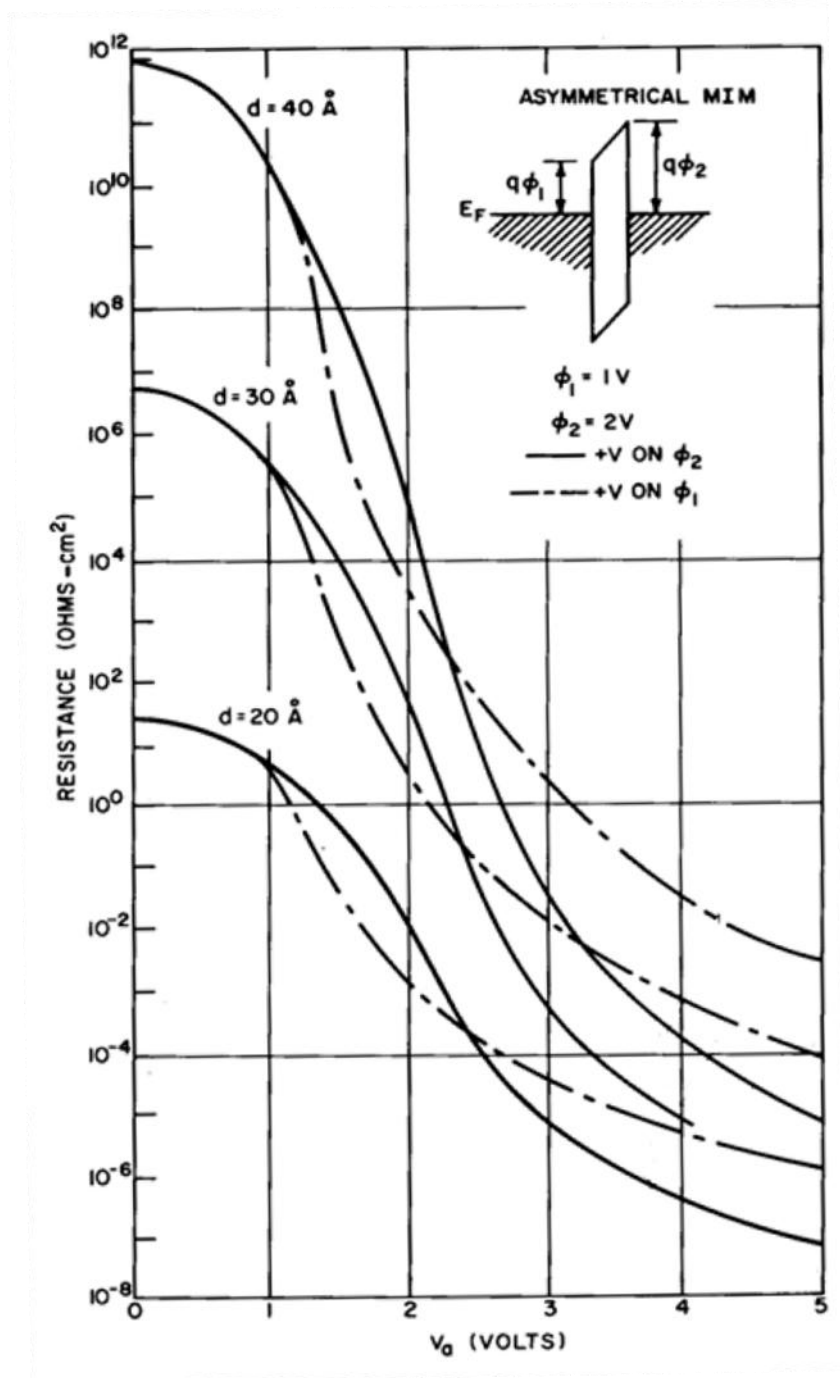


Figure 1.6: Theoretical tunnel resistance as a function of applied voltage for an asymmetrical MIM structure [7]

Another factor is the short response time for high-speed rectification. The MIM diode is one of tunneling devices. The tunneling transit time should be analyzed to achieve the high operating frequency. If the tunneling transit time is longer than the period time of incoming

wave, the device fails to efficiently rectify the incoming wave. For that of the MIM diode, RC (resistance-capacitance) constant time decides mainly the tunneling transmit time. Therefore, the capacitance and resistance should be low. The capacitance is proportional to the surface area [10, 11]. Thus the area has to be kept as small as possible. The following section explains it more detail.

1.1.3.4 Theoretical Model of the MIM Diode

An equivalent circuit of the MIM diode is shown in Figure 1.7. This model of the MIM diode can be described by a capacitance (C_D) connected parallel to a fixed resistor and a non-linear resistor (totally R_D). The fixed resistor expresses the internal resistance of the MIM diode and non-linear resistor indicates the voltage-dependent resistance.

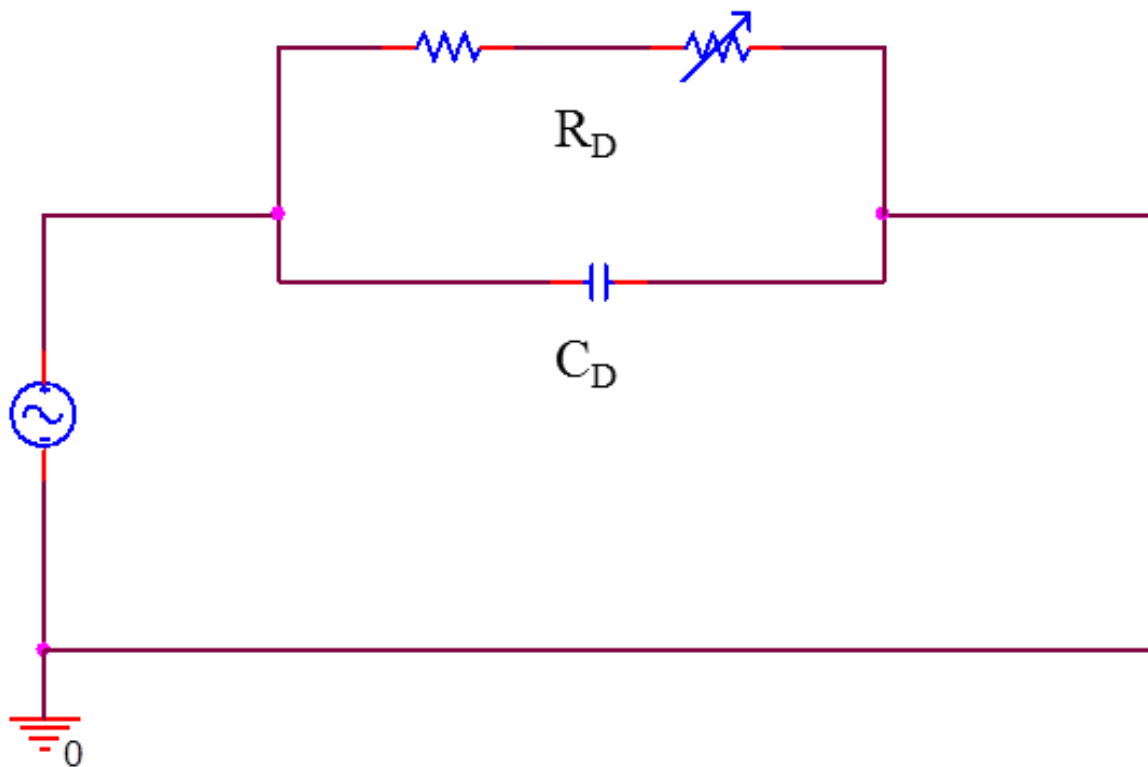


Figure 1.7: An equivalent circuit of MIM diode

The current flow passed through the capacitor and the resistance (R_D) reduces in this equivalent circuit so that the capacitance (C_D) and the resistance should be kept small. The cut-off frequency is defined as:

$$f_c = \frac{1}{2\pi R_D C_D}$$

where f_c is the cut-off frequency, R_D is the total resistance of the diode, and C_D is the capacitance of the diode. The cut-off frequency is one of the important factors to express high-speed operation, which indicates limited frequency of this device. To increase that of this device, R_D and C_D must be small, as shown in above equation. The capacitance is defined as:

$$C_D = \frac{\epsilon_0 \epsilon_r A}{d}$$

where ϵ_0 is the vacuum permittivity, ϵ_r is the relative permittivity, A is the contact area, d is the insulator thickness. According to above equation, the capacitance is mainly affected by the contact area and the thickness of insulator layer. The oxide layer thickness decides the tunnel resistance so that the capacitance of the MIM diode is generally defined by the contact area. Thus, in order to increase operating frequency of the MIM diode, it should be small. The resistance also affects to the operating frequency; therefore, it is essential to consider the resistance. The resistance is defined as:

$$R_D = \rho \frac{L}{A}$$

where ρ is the resistivity, L is the length, A is the contact area. Increasing the thickness d of insulator layer or reducing the contact area can obtain the small capacitance. If the thickness of the dielectric layer is increased, the non-linearity of I-V characteristics and the probability of tunneling are decreased. However, according to resistance equation, the big contact area and short length affect to decreasing the resistance. The contact area effect is proportional to capacitance and inversely proportional to resistance. In other words, its two parameters have trade-off relation so that the resistance and the capacitance cannot decrease simultaneously. Therefore, the optimized capacitance and resistance, the novel technique and structure to overcome the trade-off, or finding new material are required to achieve high-speed rectification.

The tunneling probability is described by the barrier height and width. The transmission probability is given by the modified Schrodinger Wave equation,

$$P = e^{-2d\sqrt{\frac{2m(V-E)}{\hbar^2}}}$$

in which P is the transmission probability, d is the thickness of the dielectric, m is a mass of the electron, V is the barrier height, E is the energy of the electron. According to this equation, the high transmission probability can be obtained by thin dielectric layer, low barrier height. The main factor to increase the tunneling probability is the thickness of the dielectric layer, as shown as above equation [10].

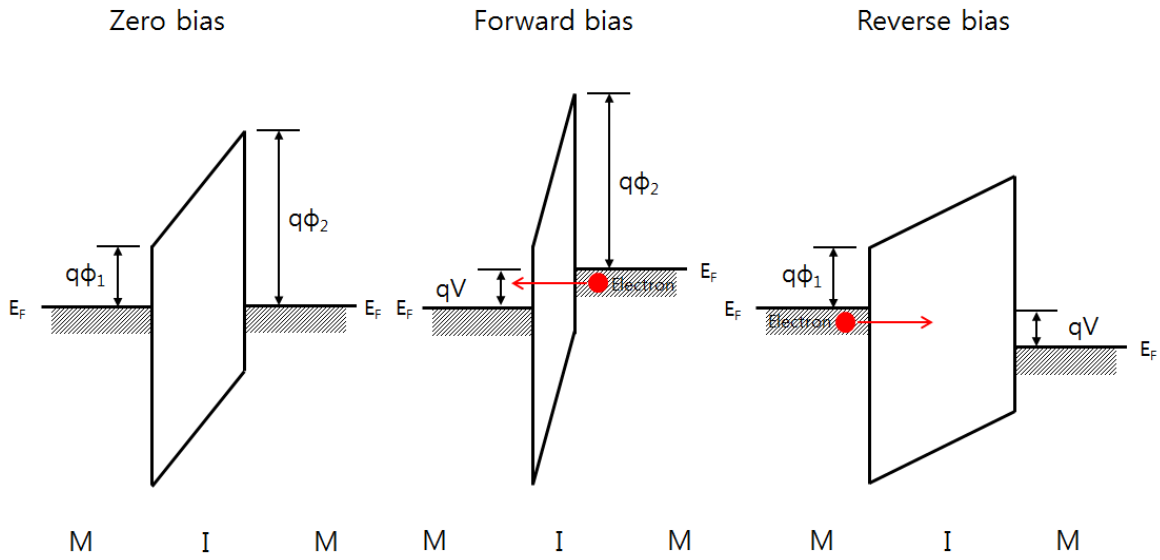


Figure 1.8: Schematic energy band diagram of MIM diode at each bias condition

Figure 1.8 illustrates the change of band gap diagram of the MIM diode at each bias condition, zero bias, forward bias, and reverse bias. The electrons can be moved to opposite metal in forward bias and reverse bias applied. Even though the same size bias applies to left metal and right metal in forward and reverse state, the tunneling probability of asymmetric MIM diode is different between forward and reverse bias applied due to change of thickness of the tunnel barrier in Figure 1.8. At forward bias applied, the thickness of the tunnel barrier is thinner so that the tunneling probability is higher than reverse bias applied. This effect is similar with control of thickness of the tunnel barrier. It indicates that large different work function makes much higher degree of asymmetry in the I-V curve.

1.1.3.1 Factors limiting MIM diode

The MIM tunneling diode is one of the high-speed rectification devices, which convert high frequency AC signal to DC signal. In order to operate at THz level, certain factors are considered to achieve high-speed operation. According to transmission line theory, parasitic capacitance exists especially at high frequency. Designing a MIM structure should be taken account of effect of the parasitic capacitance to be minimized. For I-V characteristics, the MIM diode should be non-linear and asymmetry in I-V characteristics regardless of external bias applied. The efficiency of rectification is affected by this factor. To achieve a zero bias response diode, MIM diodes are composed of different two metals that have large difference work function instead of using same metals. Also the leakage current is important for that of MIM diode. The leakage current and different work function should be considered for asymmetric I-V characteristics, related to conversion efficiency. Another factor related realization is the CMOS compatible, integration, and stability. The integration and stability issues are mainly from fabrication process.

1.1.3.2 Structure Tendency of MIM Diode

Recently, various types of MIM diodes have been studied for high-speed rectification with high efficiency. For initial point contact diode, Cat-whisker diode, a sharp tungsten wire is used to get much smaller contact area due to lack of fabrication technique to decrease size up to sub-micron. This device serves as high frequency diode. However, because of instability, its structure was changed to be more stable, “edge metal-oxide-metal (MOM) diode.” Figure 1.10 shows the schematic illustration and SEM image of edge MOM diode. This structure is more stable structure than the point contact Cat-whisker structure. It utilizes edge of metal forming thin native oxide between flat metal and perpendicularly bent metal [8]. As developing fabrication technique, a vertically simple structure as small as several nano-

meter was widely used for high-speed operation [9]. Figure 1.9 shows the TEM image of the simple structure. The MIM diode is promising structure to achieve much higher frequency with nonlinear and asymmetric I-V curve from two dissimilar metals. Therefore, the MIM structure can approach THz region.

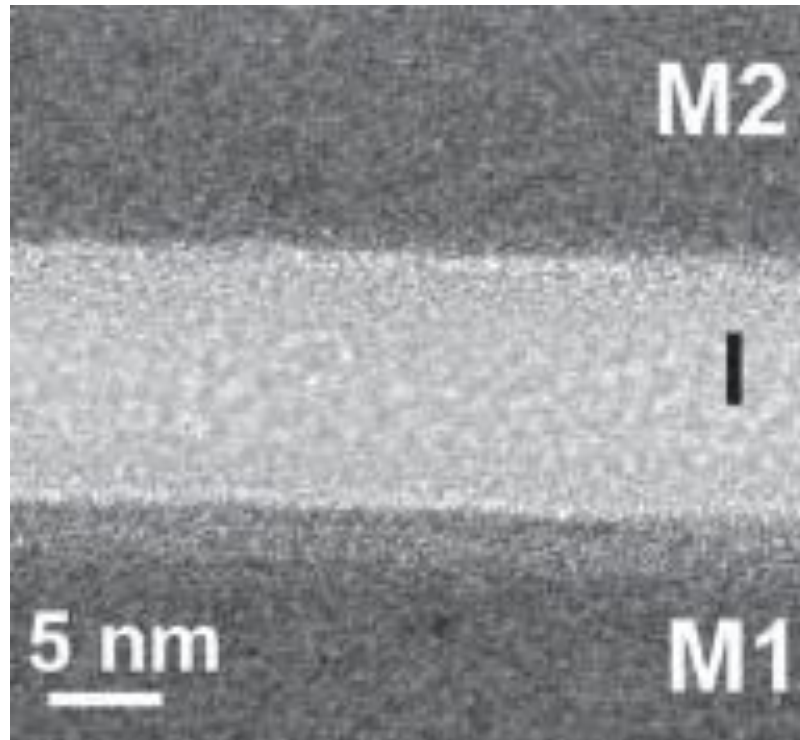


Figure 1.9: The TEM image of the simple MIM diode [12]

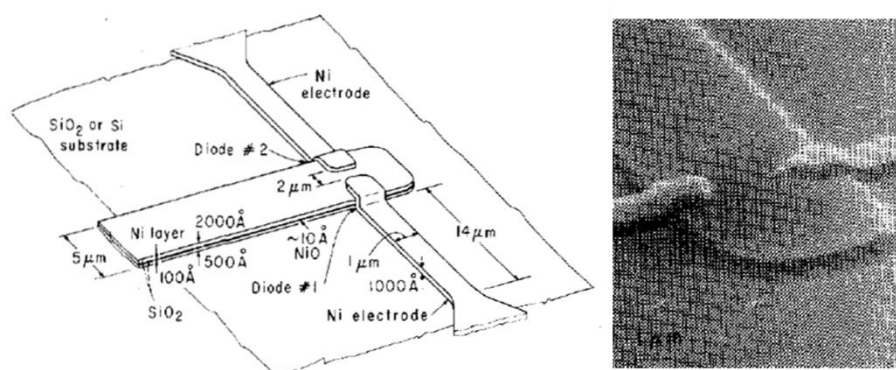


Figure 1.10: The schematic illustration and SEM image of edge metal-oxide-metal (MOM) diode [8]

1.1 Objective

The objectives of this research work in developing asymmetric metal-insulator-metal diodes were.

- High-speed rectification: The speed of rectification depends upon RC (resistance-capacitance) constant time. Short RC constant time leads to fast response time so that it can increase the operating frequency. For small capacitance, the size of contact area of the MIM diode should be small. For small resistance, the thickness of insulator within contact area also has to be thin. The probability of tunneling of MIM diode relies on these two processes, small contact area and thin insulator layer.
- Non-linearity and asymmetric I-V characteristics: For the asymmetric I-V characteristics, unidirectional behavior, selection of materials based on work function should be considered. In order to make quantity of current to be different between two directions in MIM diode, large work function difference between two materials has to be chosen.
- Structure of MIM diode: The large work function difference is not enough to serve as diode. In order to get more asymmetric I-V characteristics, structural effect should be added to the MIM diode. The sharp tip or high aspect ratio structure are utilized for field emission (FE) effect in MIM diode. High FE structure can make more asymmetric I-V characteristics for achieving high conversion efficiency.

II. FABRICATION

The three kinds of the MIM diodes, simple MIM diode, lateral MIM diode, MIC (metal-insulator-carbon nanotube) diode, are fabricated to compare the performance and the characteristics. In this chapter, the fabrication processes for three kinds of MIM diode are discussed in detail.

2.1 Fabrication of simple MIM diode

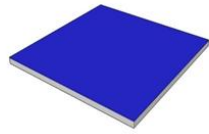
This structure is easy to be fabricated compared with the other structures due to relatively simple structure. The simple MIM diode was fabricated on Si/SiO₂ (1000 Å) to prevent the devices from unexpected leakage current that leads to low performance. We design four kinds of the simple MIM diode structures to investigate the size effect. The contact area sizes of the four sets are 10 um X 10 um, 15 um X 15 um, 20 um X 20 um, and 25 um X 25 um. There are three different material combination, Al-AlO_x-Al, Ni-NiO_x-Ni, and Al-AlO_x-Pt, to investigate the effect of that, as shown in Table 2.1.

Table 2.1: The description of the samples of simple MIM diodes

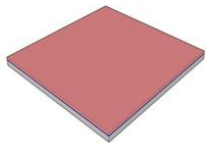
Samples	Material combination	Size of contact area
Sample #1	Al-AlO _x -Al	10 um X 10 um (3 EA)
		15 um X 15 um (3 EA)
		20 um X 20 um (3 EA)
		25 um X 25 um (3 EA)
Sample #2	Ni-NiO _x -Ni	10 um X 10 um (3 EA)
		15 um X 15 um (3 EA)
		20 um X 20 um (3 EA)
		25 um X 25 um (3 EA)
Sample #3	Al-AlO _x -Pt	10 um X 10 um (3 EA)
		15 um X 15 um (3 EA)
		20 um X 20 um (3 EA)
		25 um X 25 um (3 EA)

Before starting the fabrication, cleaning the Si/SiO₂ substrate with dipping into acetone for 60 seconds and then IPA for 30 seconds was carried out, sequentially, with ultrasonic agitation. The fabrication processes of the simple MIM diodes are defined as in Figure 2.1.

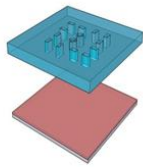
Bottom electrode



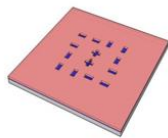
Si/SiO₂ wafer



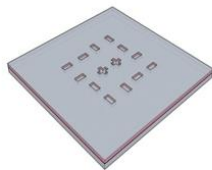
Spin coating with GXR-601 photoresist and soft bake



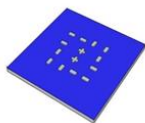
UV exposure



Developing

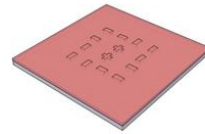


Metal deposition

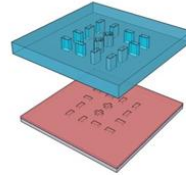


Lift-off with acetone

Top electrode



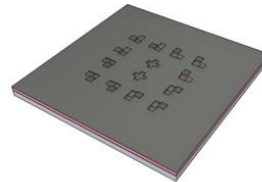
Spin coating photoresist and soft bake



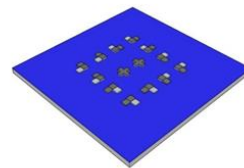
UV exposure



Developing



Metal deposition



Lift-off with acetone

Native oxidation



Figure 2.1: The whole process steps of the micro-scale MIM diode

After cleaning process the spin coating was carried out with AZ GXR-601 positive photoresist (PR) onto the Si/SiO₂ substrate. The 1500 rpm of spin speed was used to get approximately 1.5 μm of thickness of the PR. Then, the soft bake was performed with 100 °C for 60 seconds on hot plate. The wafer was exposed by the 40 mJ/cm² of UV from mercury lamp. The exposed wafer was submerged into AZ 300 MIF developer for approximately 60 seconds. Thermal and electron beam (E-beam) evaporator and sputtering system were used to deposit the materials onto the Si/SiO₂/patterned PR substrate. The materials of aluminum and nickel (4N and 4N5 of purity) were deposited by the thermal evaporator system with the ratio of 1 Å/second due to relatively low melting temperature of that; however, the high melting temperature of the platinum (4N of purity) is one of the reasons of employing the RF sputtering instead of the thermal evaporation system. After metal deposition, continuously the lift-off was carried out with acetone to obtain final bottom electrode. The lift-off can be affected by how to be performed, depending on material, substrate, size of pattern, and so forth. However, the size of designing this pattern is not small over 10 μm ; thus, it is relatively less sensitive than that of smaller size pattern. Then we employ native oxide to form insulator layer. Aluminum and nickel are to easily get thin native oxide as 2~7 nm. The processes from spin coating to lift-off were repeated with align technique of UV photolithography step. Finally, the simple MIM diodes were completely fabricated in shown as Figure 2.2. The pattern was designed by MyCAD and exported to Gerber II format to make 5" chrome photomask.

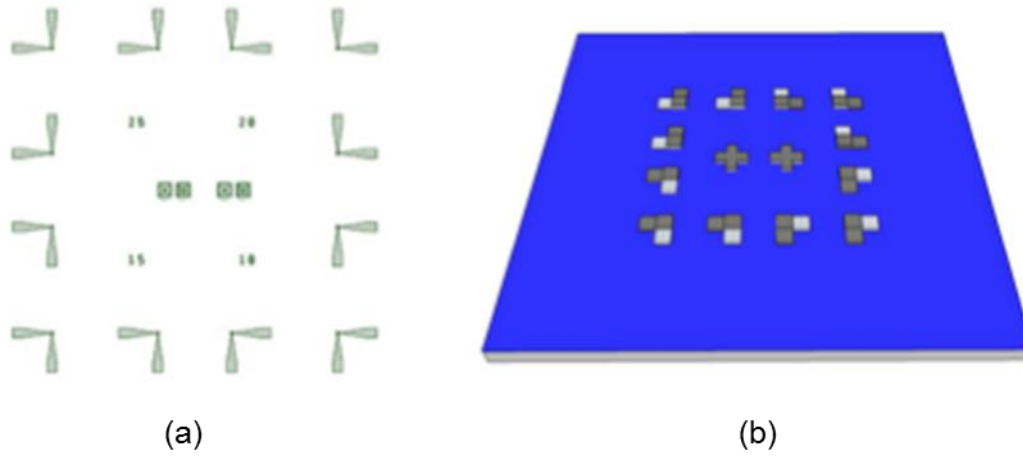


Figure 2.2: The simple MIM diode (a) the real pattern design (b) schematic illustration of the simple MIM diode

2.2 Fabrication of Lateral MIM Diode

The structure of lateral MIM diode is similar with the laid point contact MIM diode. The Si/SiO₂ (1000 Å) is used to block unexpected current from other path ways. We design the various lateral MIM diode structure with changing gap between two metals on Si/SiO₂ substrate. The fabrication is composed of photolithography and electron beam lithography (EBL) for pad and small lateral MIM patterns, respectively. The EBL is generally used to get fine smaller pattern. It commonly employs PMMA (polymethyl methacrylate) that is very sensitive to high energy electrons for direct write EBL. The lateral MIM diodes are defined as in Figure 2.3.

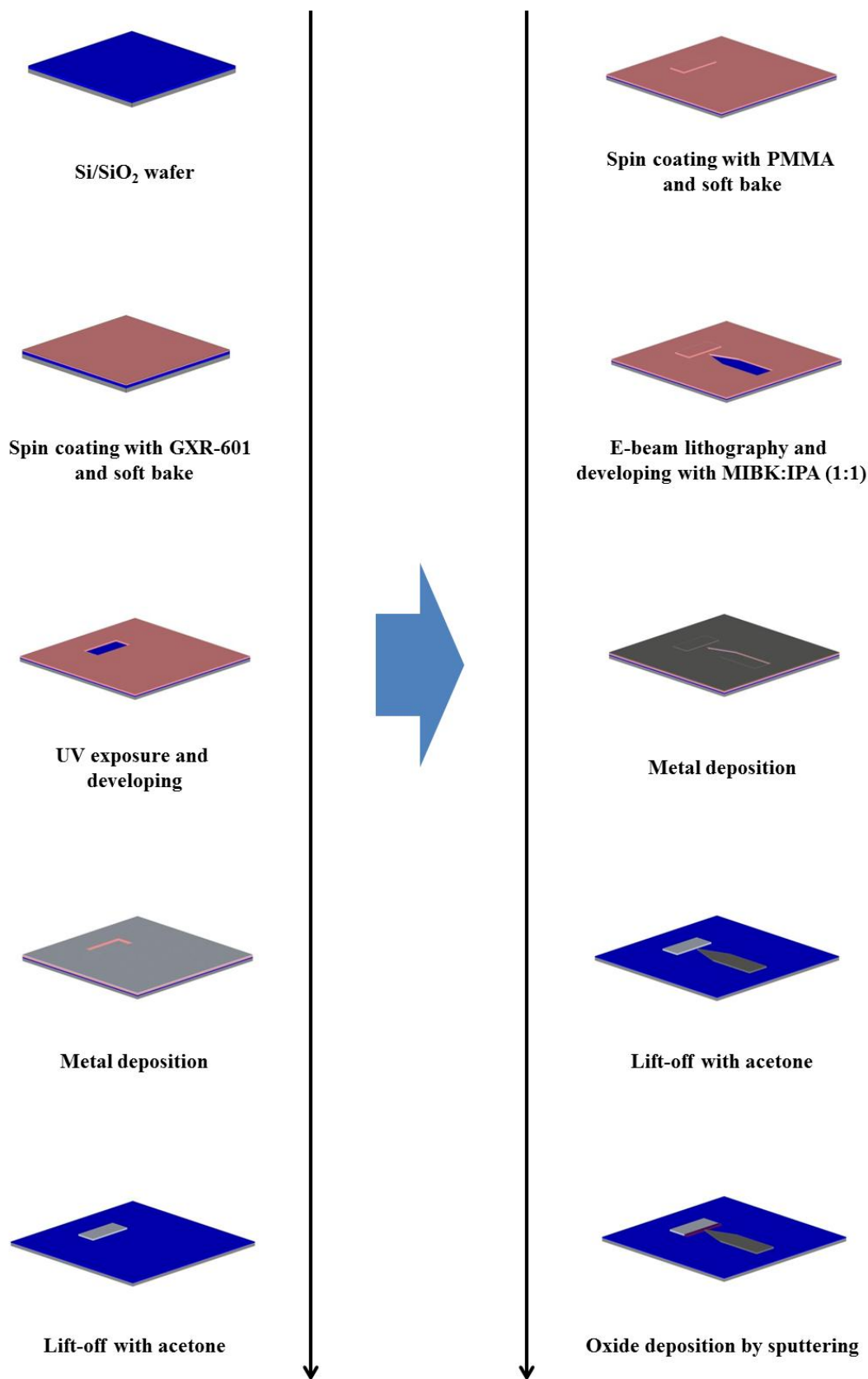


Figure 2.3: The whole process steps of the lateral MIM diode

After cleaning process the AZ GXR-601 positive PR spun on the Si/SiO₂ substrate to make bonding pad design and bottom electrode. The thickness of PR is about 1 μm with 4000 rpm of spin speed. Then, the soft bake was carried out with 100 °C on hot plate for 60 seconds. The wafer was exposed by laser writer of HIDELBURG, maskless photolithography, with 100 mW of intensity and 60 of focus. The exposed wafer was dipped into AZ 300 MIF developer for 60 seconds. The niobium of 150 nm thickness was deposited by E-beam evaporator with the ratio of 1.5 Å/sec due to high melting temperature. The lift-off was performed by submerging into acetone and then cleaning it with IPA for approximately 30 seconds. After lift-off the fabrication of bottom electrode and bonding pad, E-beam lithography pattern was carried out. For the EBL, MicroChem Corporation's PMMA A3 was used as positive electron beam resist (ER). The PMMA A3 layer was coated on a wafer with 5000 rpm for 40 seconds to obtain the thickness of 90 nm. The sample was baked for 300 seconds on a hotplate at 170 °C. The EBL was carried out using a JEOL JBX-9300 Electron Beam Lithography System. This system generally operates with 100kV of acceleration voltage and 1 nA of current. For our devices, we used 300 $\mu\text{C}/\text{cm}^2$ as optimized dose with alignment between bonding pad and bottom electrode. The development was then carried out with the ratio of 1:1, methyl isobutyl ketone (MIBK): IPA, for 180 seconds. The titanium and platinum were deposited by RF sputtering, 5 nm and 45 nm, respectively. Following that the lift-off was performed with acetone. The thin oxide layer as thin as 20 nm was formed by RF sputtering (at 1×10^{-2} torr of process vacuum) to the whole area.

2.3 Fabrication of Metal-Insulator-Carbon nanotube Diode

The MIC diode is a kind of point contact structures, similar with “Cat-whisker diode”. However, this structure not only has smaller contact area and higher aspect ratio from the structure of a CNT, but also overcomes the mechanical instability using vertical growth

technique with sustaining by SU-8 polymer. The Figure 2.4 and 2.5 show the whole process step of the MIC diode, 3D and cross-section view.

After cleaning process the spin coating was performed with AZ GXR-601 positive PR on the Si/SiO₂ substrate to form bottom electrode. The thickness of PR is about 1 μm with 4000 rpm of spin speed. Then, the soft bake was carried out with 100 °C on hot plate for 60 seconds. The wafer was exposed by laser writer of HIDELEBURG, maskless photolithography, with 100 mW of intensity and 60 of focus. The exposed wafer was dipped into AZ 300 MIF developer for 60 seconds. The 150 nm of niobium was deposited by E-beam evaporator with the ratio of 1.5 Å/sec. The lift-off was performed by submerging into acetone. After lift-off the fabrication of bottom electrode was completed. And a cycle of this fabrication based on photolithography and lift-off was repeated to form oxide layer and contact pad opening. The PMMA A3 layer was applied to the sample after lift-off using a wafer spinner at 5000 RPM for 40 seconds to obtain the thickness of 90 nm. The sample was baked for 300 seconds on a hotplate at 170 °C. In fabrication of the MIC diode, the EBL was carried out using a JEOL JBX-9300 Electron Beam Lithography System to compose the catalyst, 100 nm, to grow a CNT. The 400 $\mu\text{C}/\text{cm}^2$ was used as optimized dose with alignment on the selected area. The development was then carried out with submerging the developer including ratio of 1:1, MIBK: IPA, for 180 seconds. The 20 nm of nickel as the catalyst for a CNT was deposited by RF sputtering. Then, the lift-off was carefully performed by just agitation by hand due to small size of pattern. After formation of the catalyst, the PECVD, Black Magic 2 inch system of AIXTRON, was carried out to vertically grow a CNT with C₂H₂/NH₃ gas flow, 600V of plasma intensity, 650 °C of temperature, and 10 minute of growth time on patterned nickel catalyst position. After the growth of a CNT on selected location, the spin coating is performed with SU-8 2002 negative PR at 4000 RPM for 1.5 μm thickness to prevent a CNT from mechanical instability and sustain the top electrode. The sample was baked on a hot

plate with 95 °C for 90 seconds. The sample was then exposed by UV with a dose of 70 mJ/cm². The development was carried out using SU-8 developer for 60 seconds. The thin PR layer on CNT was removed using O₂ plasma for 30 seconds to connect with top electrode, in sequence. The hard bake is consisted of two steps. As first step the temperature increased from 20 °C to 150 °C for 300 seconds to prevent SU-8 polymer from stress and deformation, and then kept 150 °C for 300 seconds. Following this process, the AZ GXR-601 positive PR spun onto the hard-baked SU-8 2002 PR to make top electrode. The sample was exposed with higher dose (60 mJ/cm²) due to partial change of profile of the substrate and the development was same as previous AZ GXR-601 condition. The aluminum was deposited by thermal evaporator to easily get lift-off. The lift-off was carefully performed because the adhesion between hard-baked SU-8 2002 and aluminum is not good. The yield almost depends on the last lift-off process. The MIC diode was completely fabricated, as shown in Figure 2.6.

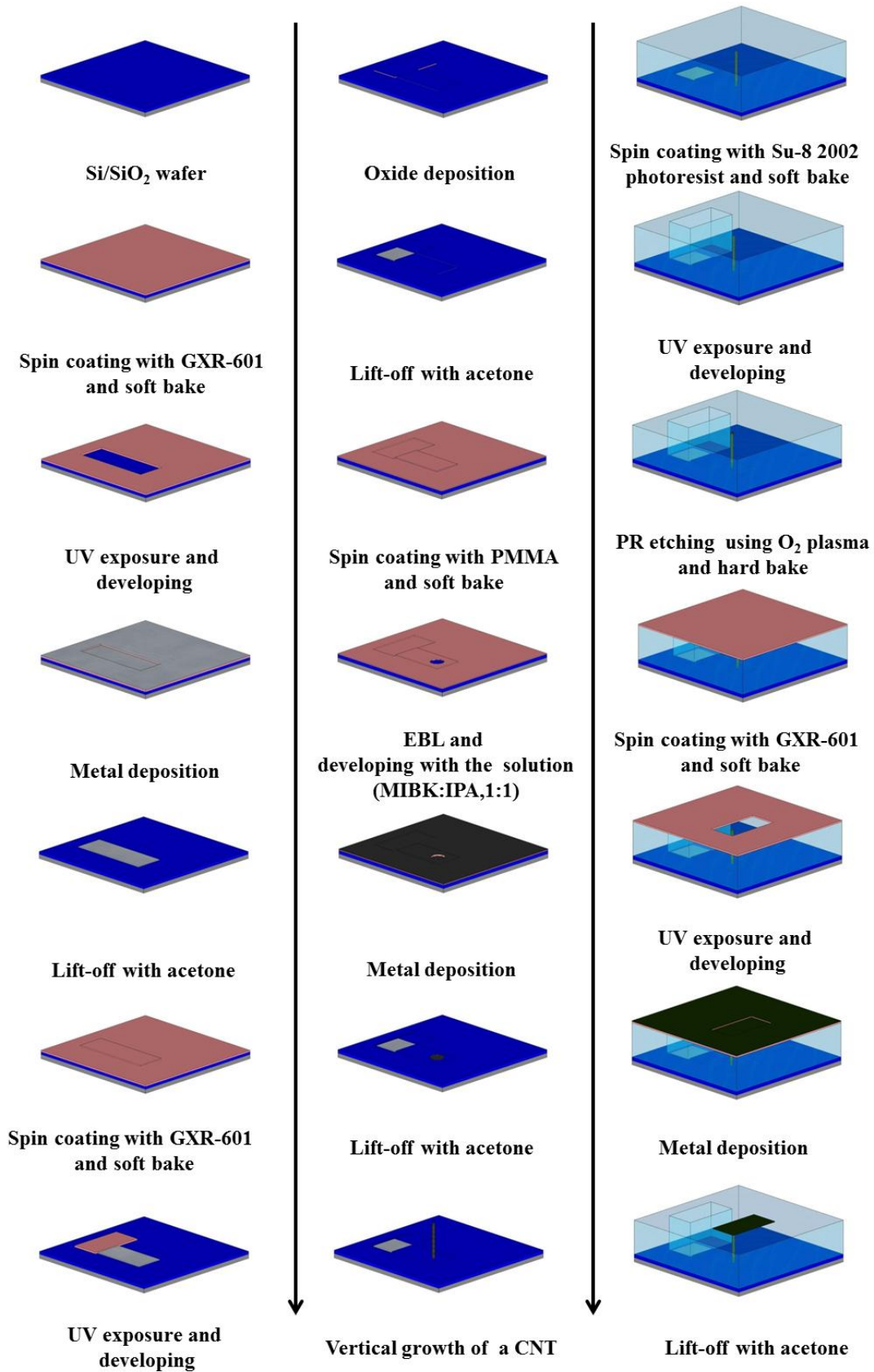


Figure 2.4: The whole process steps of the MIC diode (3D view)

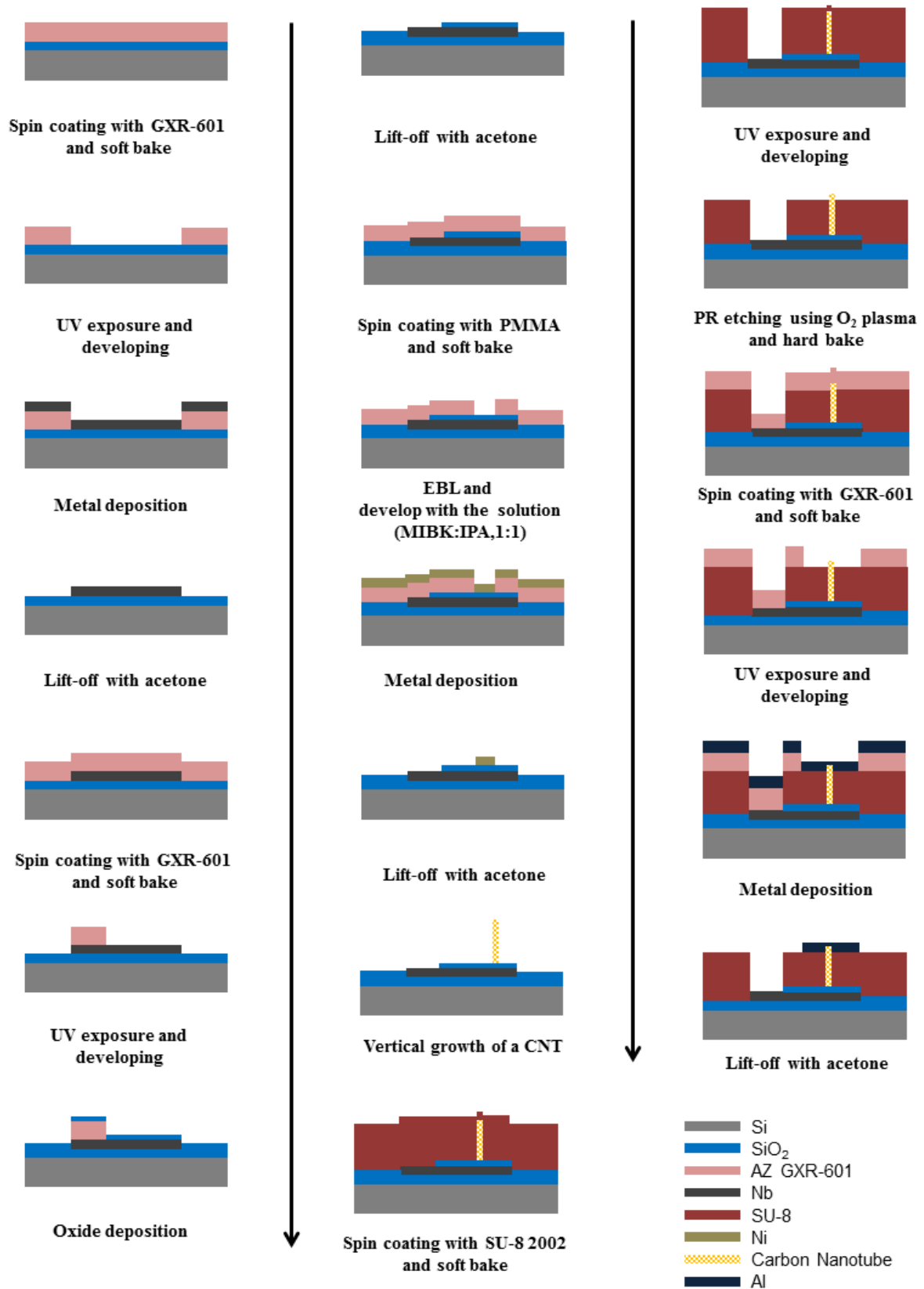


Figure 2.5: The whole process steps of the MIC diode (Cross-section view)

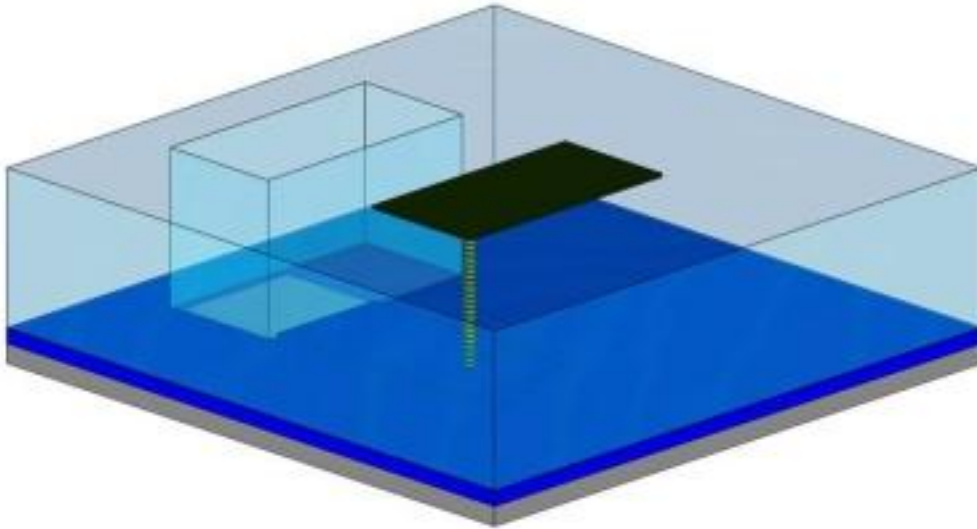


Figure 2.6: The schematic illustration of MIC (metal-insulator-carbon nanotube) structure

III. ELECTRIC CHARACTERISTICS AND RESULTS

3.1 Electric characteristics of simple MIM diode

A simple MIM diode has vertical sandwich structure with thin oxide layer between two metals for tunneling effect, which leads to a low threshold voltage and a high frequency. Work function difference and small junction area are the very important factors for high frequency diode. Because, the work function difference and small junction area make asymmetric I-V curve for rectification and small capacitance, respectively.

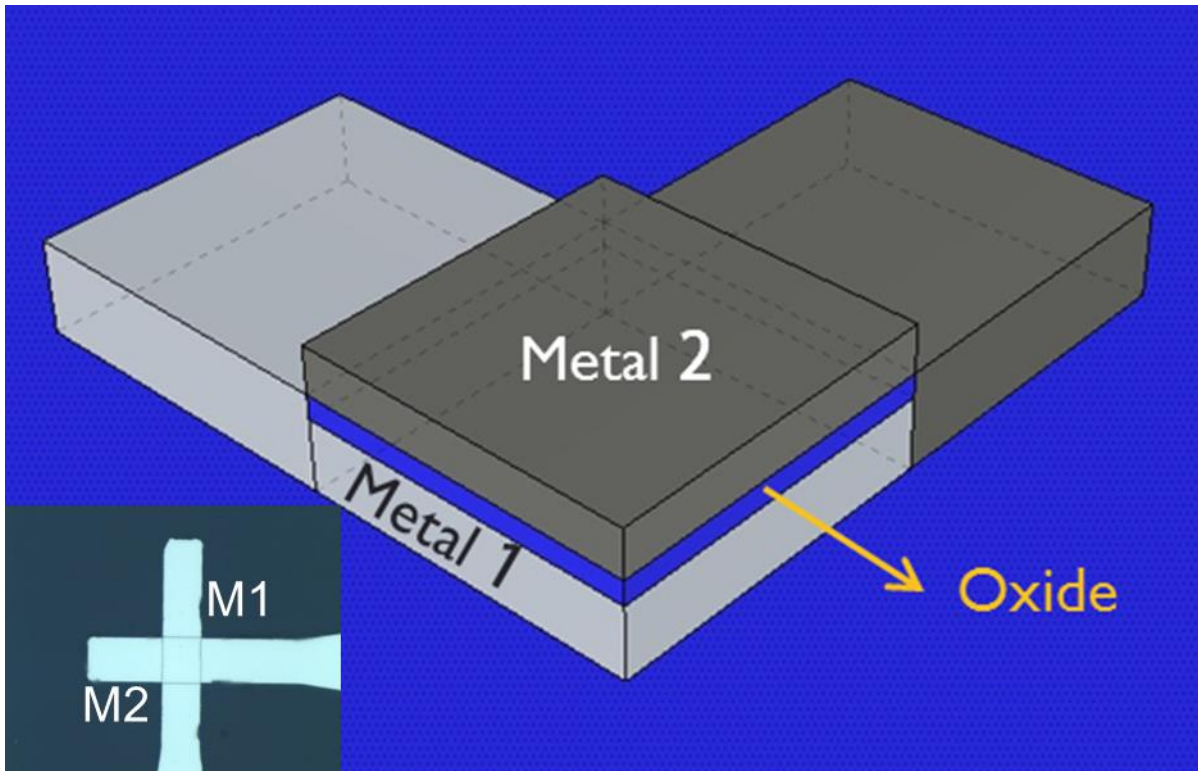


Figure 3.1: The schematic diagrams and photo image of the a simple MIM diode

Figure 3.1 shows the schematic diagrams and photo image of the symmetric structural MIM diode. These diodes are the material sets of Al-AlO_x-Al, Ni-NiO_x-Ni, and Al-AlO_x-Pt for work function difference and each material sets has four dimensional-set structure, 25 X 25 μm^2 , 20 X 20 μm^2 , 15 X 15 μm^2 , and 10 X 10 μm^2 . Although the dimension of the diode is hard to compare with nano-scale simple MIM diode due to the large difference of the scale between them, the characteristics are enough for the study.

Table 3.1: Work Functions

Materials	Work functions (eV)
Al	4.28
Ni	5.15
Pt	5.65

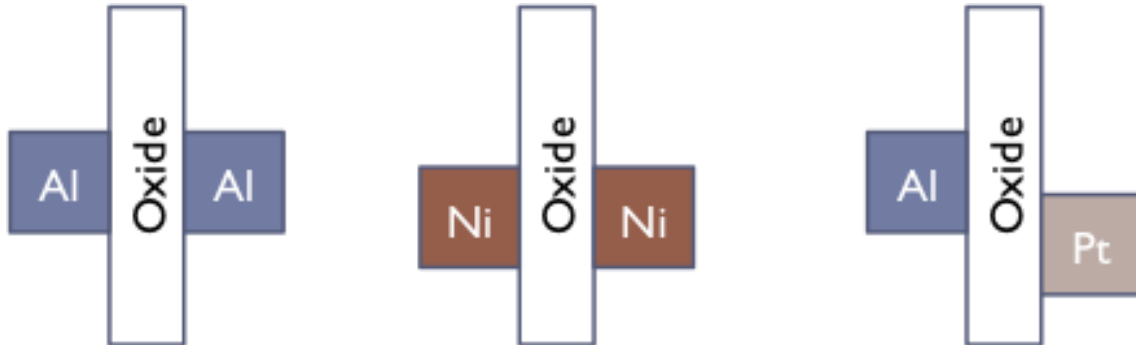


Figure 3.2: The band diagram of sets of Al-AlO_x-Al, Ni-NiO_x-Ni, Al-AlO_x-Pt

Table 3.1 shows work functions of each material, aluminum, nickel, and platinum. The combination of Al-AlO_x-Pt has asymmetrical structure. The work function differences are 0 eV and 1.3 eV for symmetrical structure and asymmetric structure, respectively, subtracting work function of aluminum from platinum. Figure 3.2 illustrates the band diagram of sets of Al-AlO_x-Al, Ni-NiO_x-Ni, Al-AlO_x-Pt. The band diagram also presents

work function difference of each material using the distance from the top of oxide to the material block.

Figure 3.3 shows the TEM image of cross-section view of Al-AlO_x-Al MIM structure. The thickness of native oxide layer is about 5.6 nm. The aluminum and nickel is easy to obtain thin native oxide layer so that these materials were used to form bottom electrode.

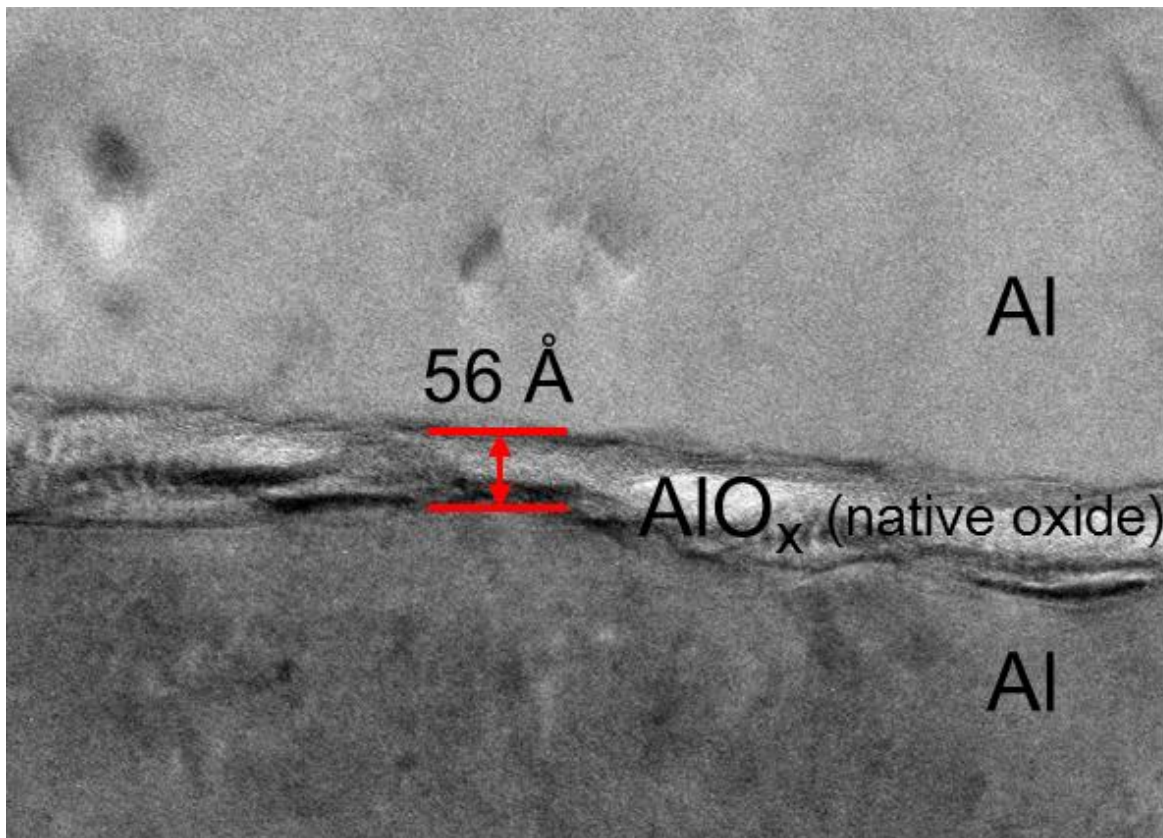
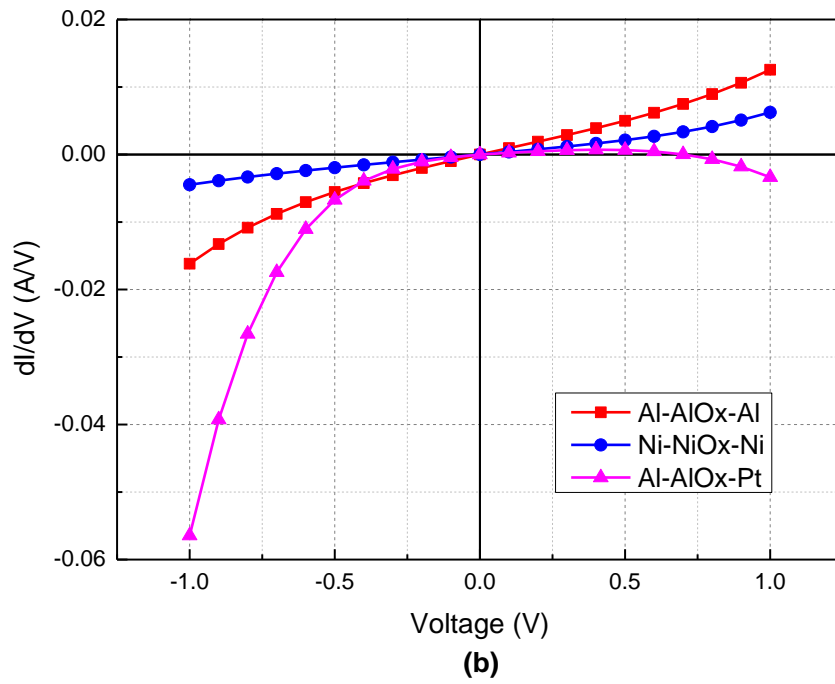
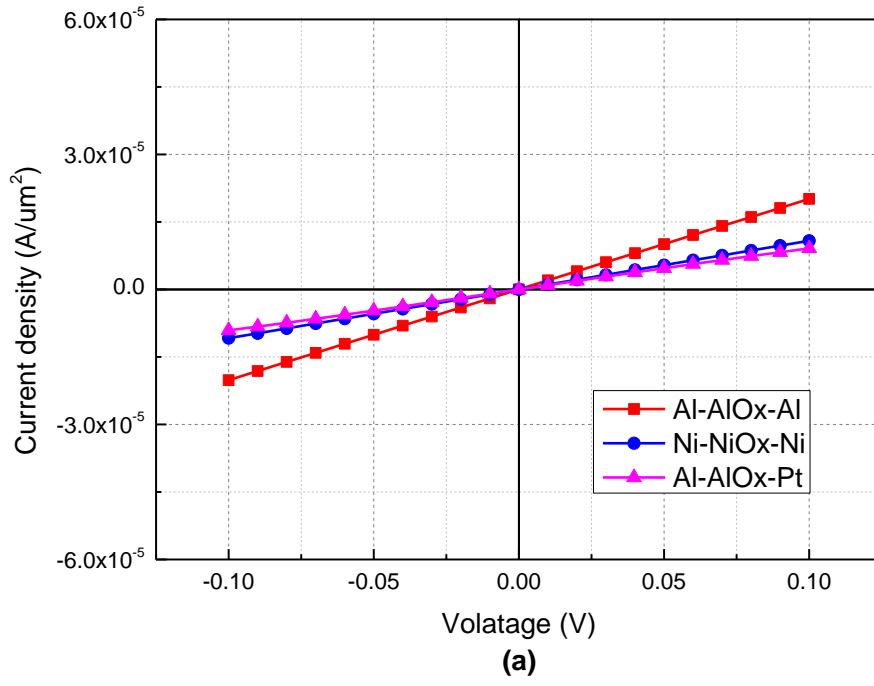


Figure 3.3: The TEM image of cross-section view of Al-AlO_x-Al MIM structure



**Figure 3.4: Electrical characteristics of the MIM structure (a) current densities of various metal contacts
(b) fifth-order polynomial fit of graph of various metal contacts**

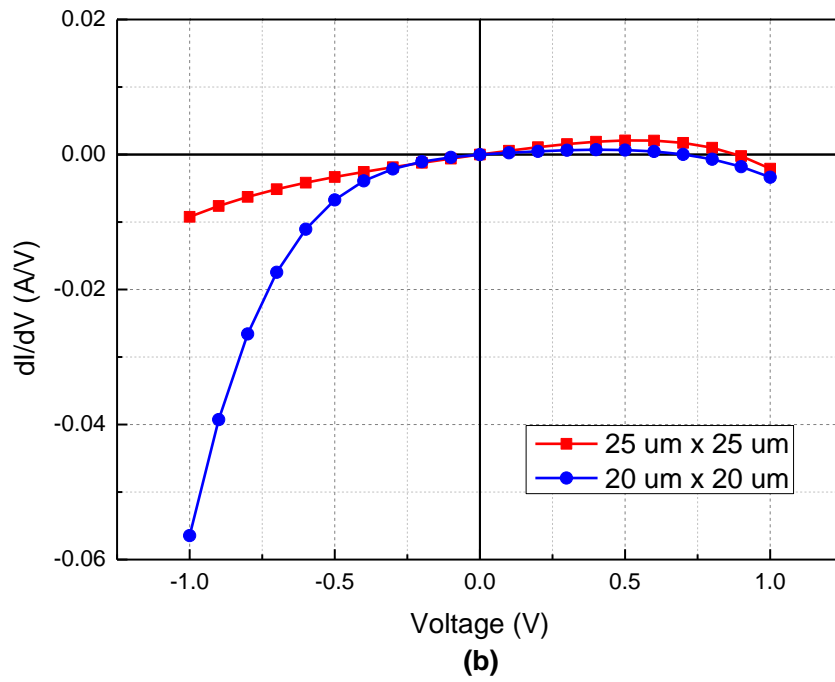
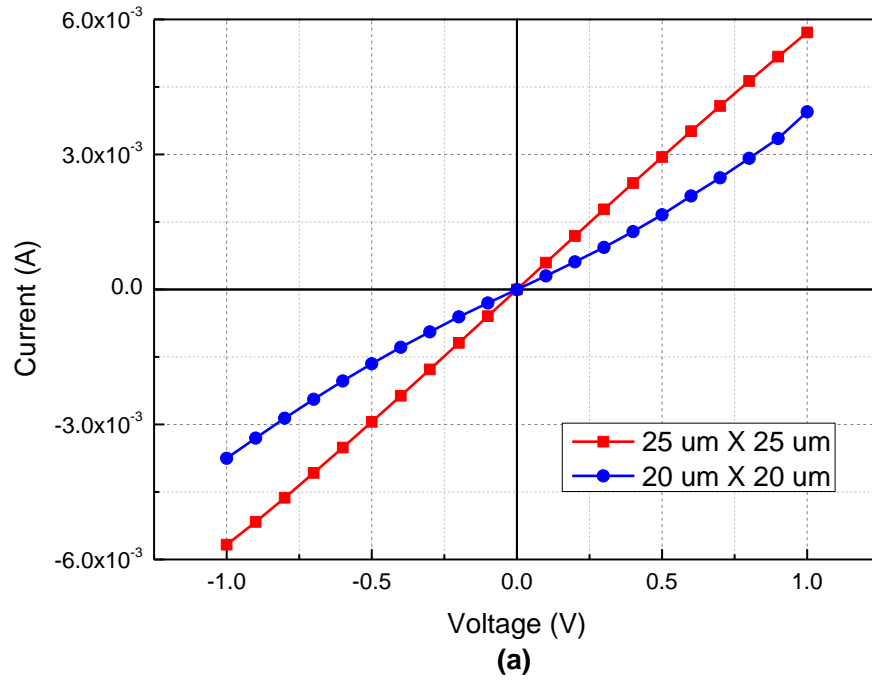


Figure 3.5: Electrical characteristics of the MIM structure (a) I-V characteristics of various size of junction area of Al-AlO_x-Pt (b) fifth-order polynomial fit

Figure 3.4 and Figure 3.5 shows the electrical characteristics of the MIM structure, current density, I-V characteristics, and polynomial fit. These values measured by Keithely 4200 SCS in DC probestation with microscope. Al-AlO_x-Al and Ni-NiO_x-Ni devices have the almost symmetrical I-V curve at negative to positive bias sweep, as shown in Figure 3.4 (a). The work function is related to the energy of the electron, which is associated with the tunneling probability; thus, the probability of tunneling is almost equal to both directions, negative and positive bias, due to the same work function of two electrodes, as shown in Figure 3.4 (a).

Even though Al-AlO_x-Pt structure makes the different barrier formations to the oxide-metal interfaces due to the difference of material work functions, the asymmetric effect of I-V curve is quite small. The contrast ratio at ± 1 V is about 1.05. Generally the work function difference among metals is below 1eV, so that it is not easy to get high rectifying effect using this MIM structure. The asymmetric phenomenon can be shown at the fifth-order polynomial fit. Since the current can flow to both directions due to the almost symmetric I-V curve, it is hard to expect the rectifying effect despite using the MIM diode structure for high frequency region. Therefore, other structures and mechanism should be considered to overcome the limits.

3.2 Electric characteristics of Lateral MIM diode

To solve the symmetric I-V characteristics, the new asymmetric MIM structure is considered. This idea is from certain experiment, the characteristics of Al-AlO_x-Probe tip structure on the Si/SiO₂ substrate with moving to Z-location, as shown in Figure 3.6.

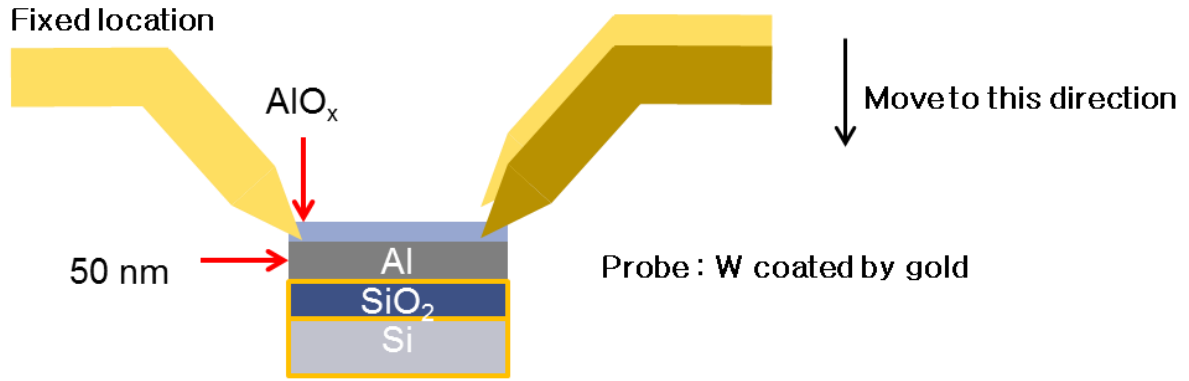


Figure 3.6: The description of the measurement of Al-AlO_x-Probe tip (Au) structure on the Si/SiO₂ substrate with moving to Z-location

The sharp tip, probe tip, is used as top electrode to investigate structure effect. Its structure is Al-AlO_x-Probe tip for structural asymmetry. The preparation of the sample is only metal deposition by thermal evaporator and spontaneously forming native oxide layer approximately 6 nm. Before measuring the characteristics, a probe tip is located onto the aluminum passed through the native oxide layer and keeps this location especially to Z-direction. Another probe tip was positioned on AlO_x layer. Then, the probe tip moves to a little bit down and we measure the I-V characteristics, repeatedly.

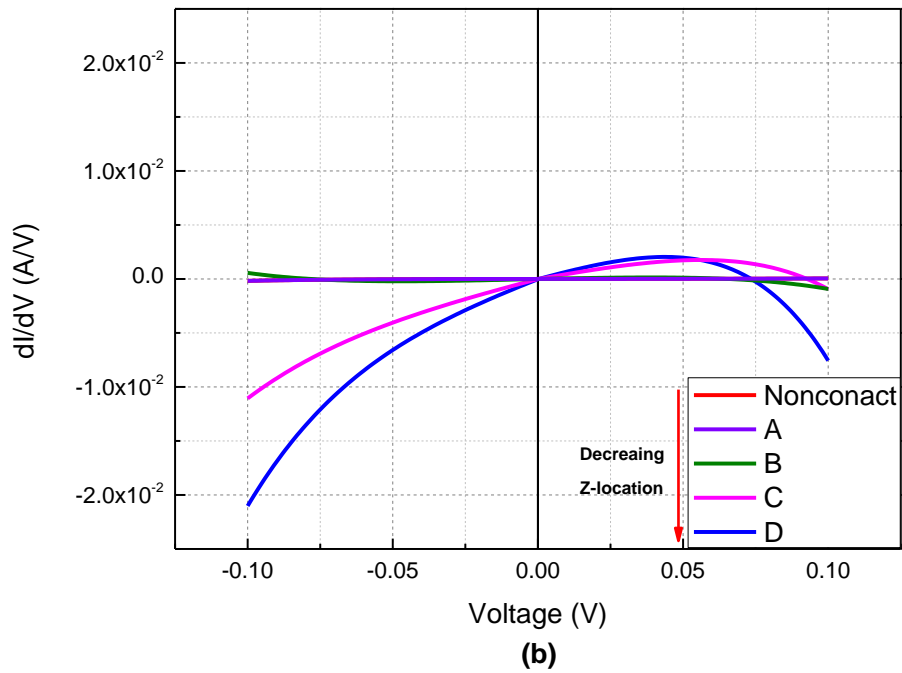
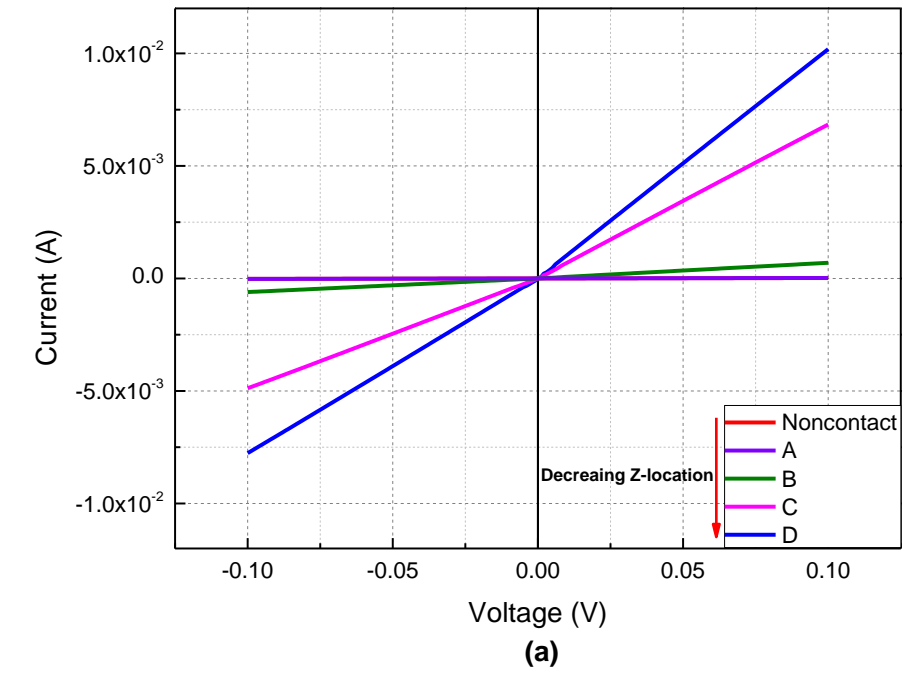


Figure 3.7: Electrical characteristics of the Al-AIOx-Probe tip structure (a) the I-V characteristics (b) fifth-order polynomial fit

Figure 3.7 shows Electrical characteristics of the Al-AlO_x-Probe tip structure, the I-V characteristics and fifth-order polynomial fit. At the position of non-contact, there is no current flow. The difference of the current flow and the asymmetric I-V curve depends upon the Z-location of probe tip. Even though the sharpness of the tip of the probe is lower, the asymmetric characteristic of I-V curve is larger than that of the structure based on work function difference. For more accurate data, another experiment was carried out using much thicker SiO₂ layer, 20 nm, as shown in Figure 3.8. Figure 3.9 shows the I-V curve of the Al-SiO₂-Probe tip structure at certain Z-location in SiO₂ layer.

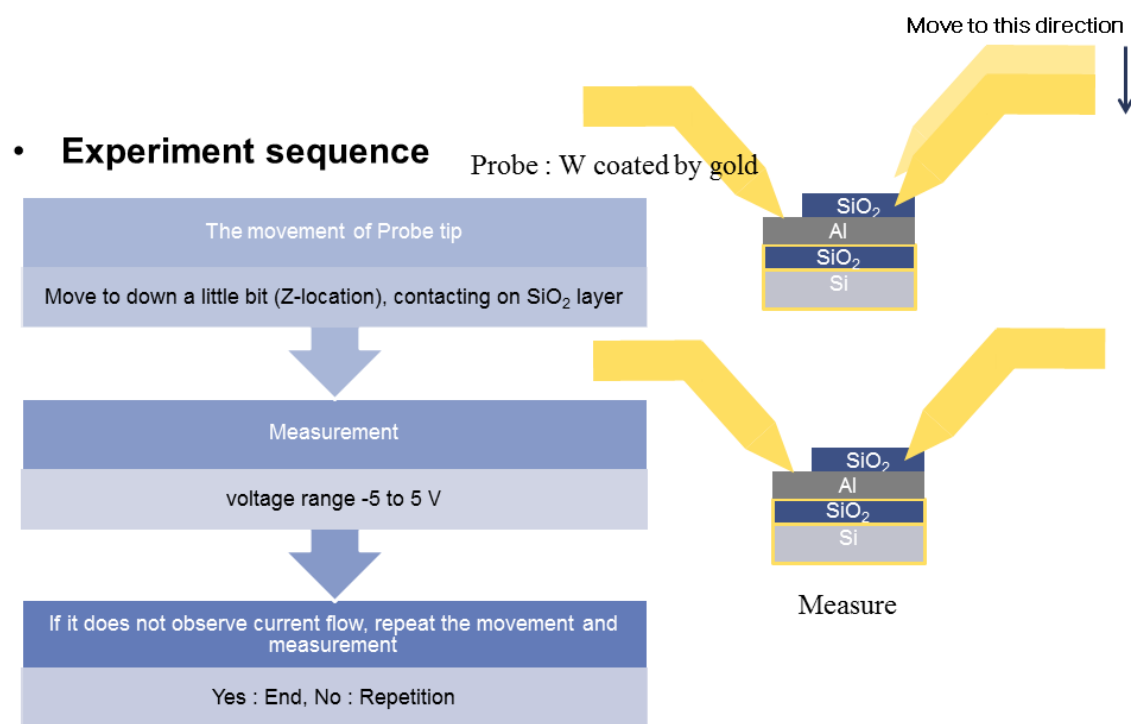


Figure 3.8: The description of the measurement of Al-SiO₂-Probe tip structure on the Si/SiO₂ substrate with moving to Z-location

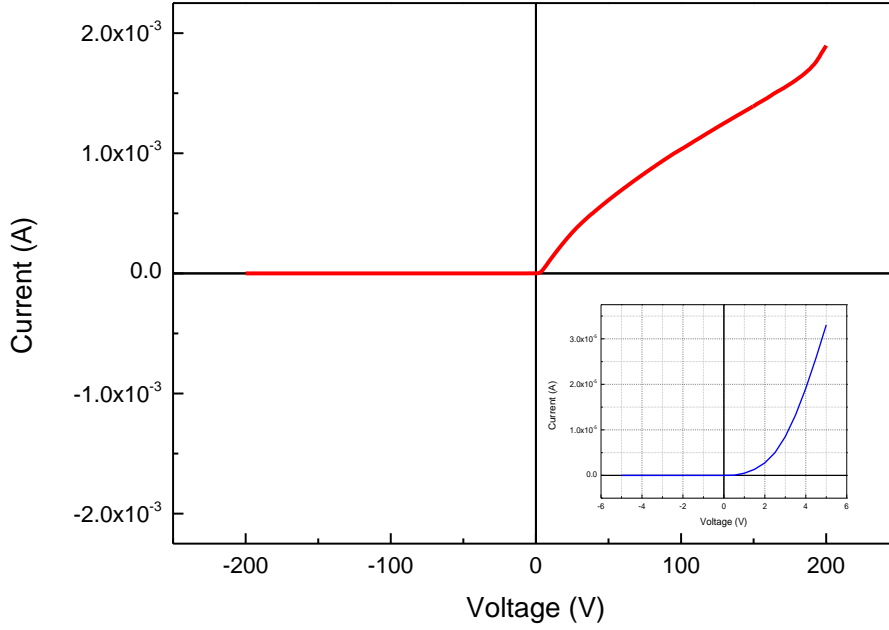


Figure 3.9: The I-V curve of the Al-SiO₂-Probe tip structure

The result of certain Z-location is good rectifying behavior from -200 V to 200 V under DC bias state. The current flow at negative region is very small, while positive region can make the current flow of mA level. Even though measurement range is too broad up to 200, the asymmetric I-V curve can be observed with much bigger order than the simple MIM structure. Based on these experiments, the different metal electrode shape can be considered to get much more asymmetric characteristics.

The sharp or high aspect ratio structure can make the large difference of potential barrier with material work functions difference. For the flat metal and the insulator under applied electrical field, the potential energy (PE) can be written as

$$PE_{M \rightarrow O}(x) = (E_F + \phi) - \frac{e^2}{16\pi\epsilon_0 x} - exE \quad (1)$$

However, if the flat metal structure is changed to sharp structure, the PE equation is also changed to including β , field enhancement factor (2).

$$PE_{M \rightarrow O}(x) = (E_F + \phi) - \frac{e^2}{16\pi\epsilon_0 x} - \beta exE \quad (2)$$

The current from sharp or high aspect ratio structure is described by Fowler-Nordhiem equation [13]:

$$J = A \frac{(\beta E)^2}{\phi} \exp\left(-\frac{\beta \phi^{\frac{3}{2}}}{\beta E}\right) \quad (3)$$

The β is mainly affected from the electrode structure. The sharp or high aspect ratio structure makes the higher β , so that the sharpness induces the higher tunneling current and the lower PE. For the ideal case, the β value can be increased to 2000 [13]. The potential energy in (2) equation can be changed with much higher order than (1) equation. Therefore, the more asymmetric I-V curve can be obtained by structure effect.

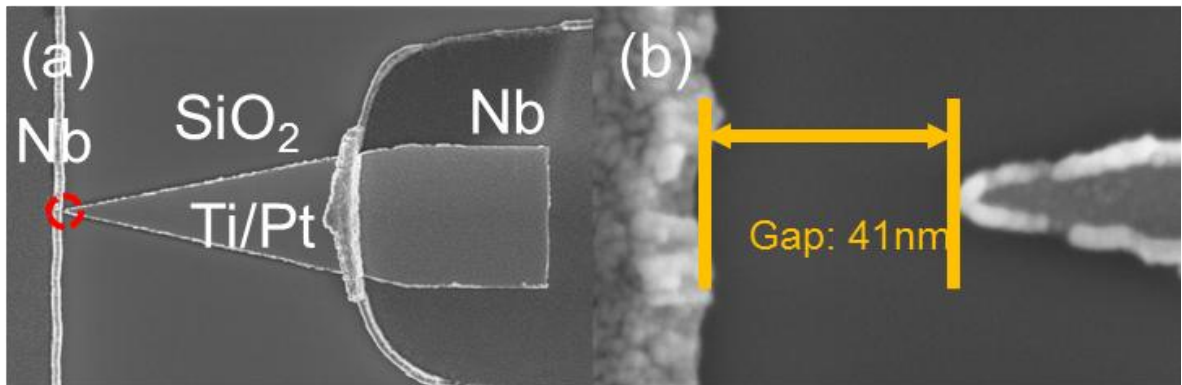


Figure 3.10: SEM image of the lateral MIM structure (a) the lateral structure with narrow gap (b) magnified view of gap of the lateral structure

To apply the idea to diodes structure, the lateral asymmetric structure is designed. Figure 3.10 shows the SEM image of the lateral MIM structure. The structure consists of flat metal and sharp tip-like structure. The lateral asymmetric structure is fabricated by E-beam lithography with very narrow gap approximately 41 nm. The structure is made of Niobium and titanium/platinum with flat structure and sharp tip, Nb-SiO₂-Ti/Pt lateral MIM diode. This structure is enough to reduce the PE as well as increase the tunneling current with high β value.

The electrical characteristics of the asymmetric lateral MIM diode are shown in Figure 3.11. These graphs show rectifying characteristics and Fowler-Nordheim tunneling plot without polynomial fit. Its threshold voltage is about 20 V. The straight line in Figure 3.11.(b) presents the evidence to induce Fowler-Nordheim tunneling over the threshold voltage range. It can be better performance as diode than the symmetric MIM diode. Although it has good rectifying characteristics and tunneling effect, the operating voltage is as high as over 20 V due to high resistance from widen the gap size, which lead to low cut-off frequency. The estimated cut-off frequency is approximately 15.47 Hz. It also is hard to precisely control the gap size and less asymmetry improvement than we expected, due to system accuracy. If it can be an ideal model, the accuracy of control of the gap is less than 1 nm.

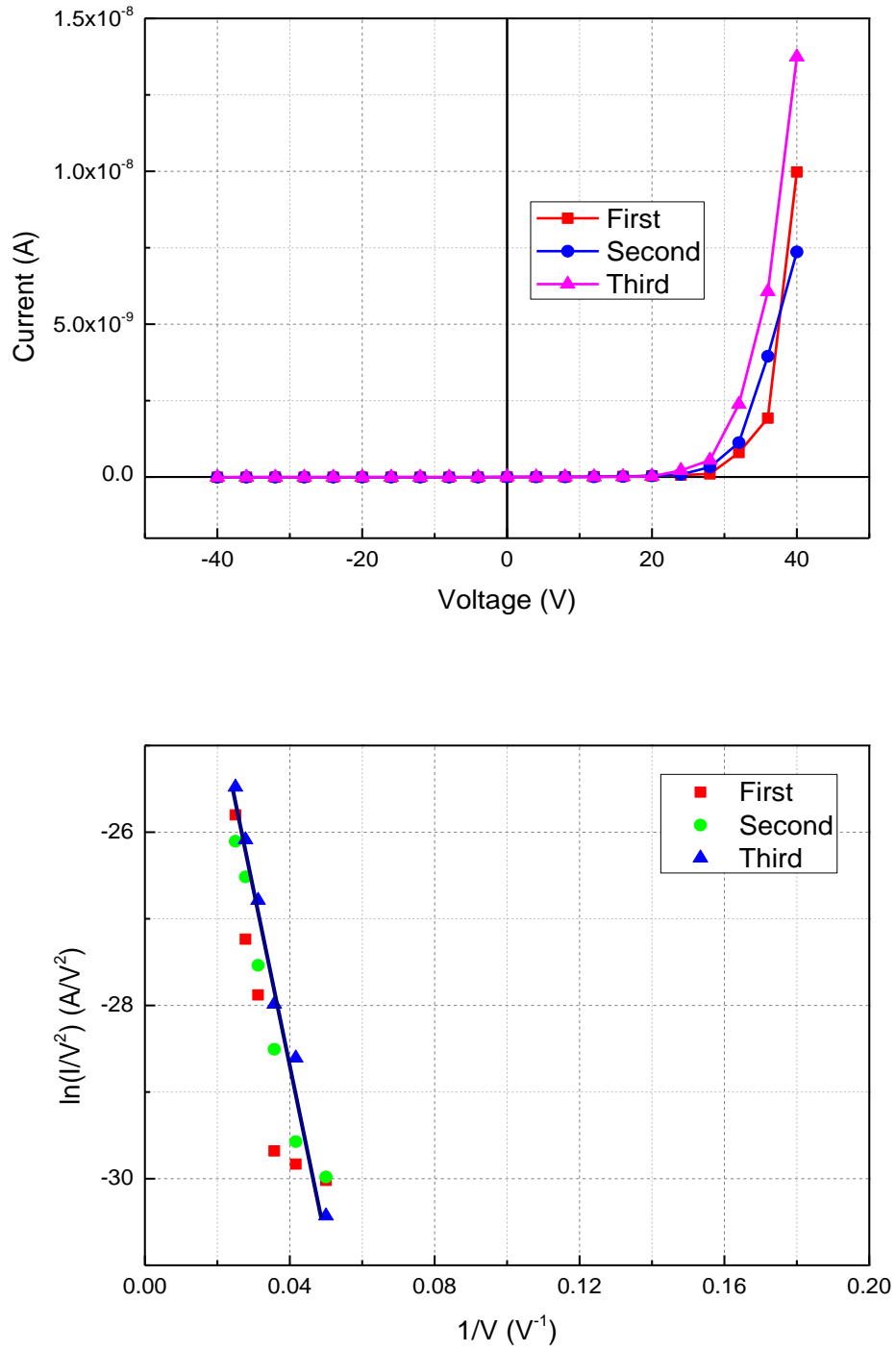


Figure 3.11: The electrical characteristics of lateral MIM diode (a) I-V curve of Nb-SiO₂-Pt lateral MIM structure with gap approximately 41 nm (b) the plot based on Fowler-Nordheim tunneling model

3.3 Electric characteristics of MIC diode

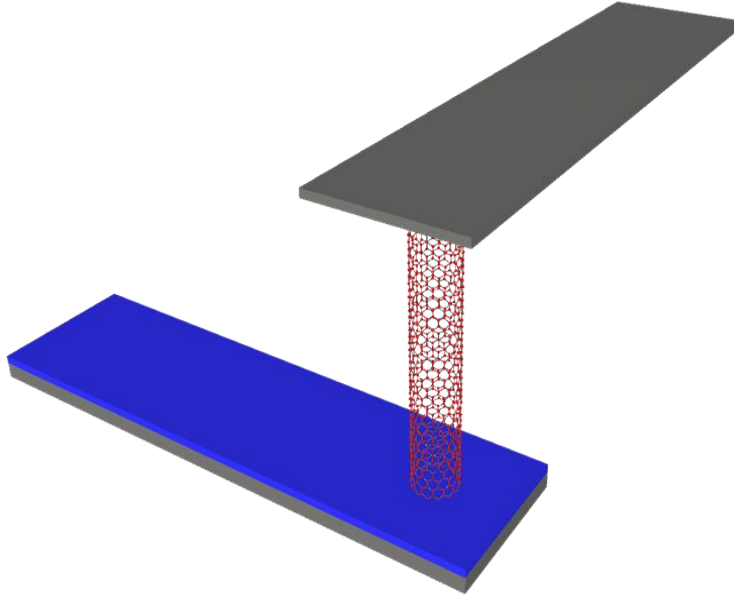


Figure 3.12: The schematic illustration of the MIC diode

To solve the problem of the lateral MIM structure, the MIC (Metal-Insulator-Carbon nanotube) structure is suggested. Figure 3.12 shows the schematic illustration of the MIC structure. The vertically aligned multi-walled carbon nanotube (MWCNT) was formed to selected position on Oxide/Metal layer. To remove the current flow between the bottom and the top electrode directly and to from electrode on top of the MWCNT, 2 μm polymer (SU-8) was coated on CNT/Oxide/Metal structure. The thick polymer prevents the current flow. The almost current flows through metal-insulator-CNT-metal pathway. For positive bias, the small sharp nano-electrode, CNT, has a high electric field density.

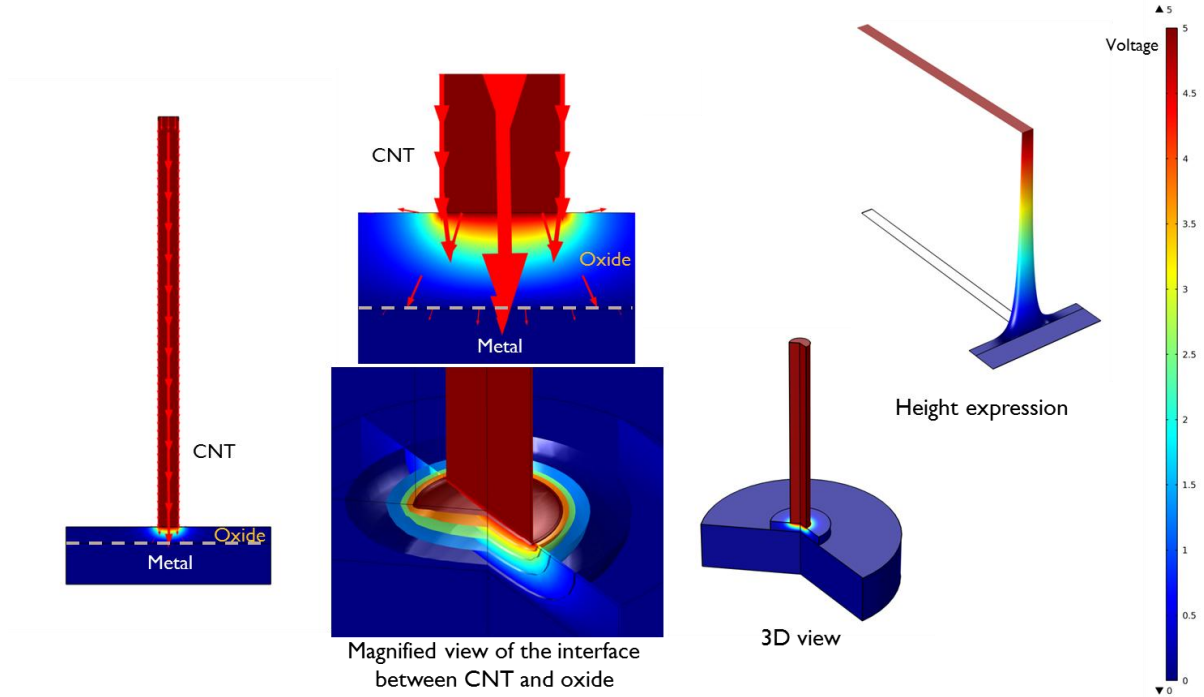


Figure 3.13: the The various simulation results based on the electric potential of the MIC structure by COMSOL

Figure 3.13 is the results of field simulation using COMSOL. The field distribution in MIC structure can be indirectly observed through various kinds of simulation results. The color presents the level of electric potential. All simulations were carried out under applied 5 V and 0 V bias to the top of a CNT and the bottom of niobium, respectively. The high aspect ratio CNT structure can induce the field emission tunneling effect. The lower potential from the high β value make the higher current flow.

Figure 3.14 shows the image after forming catalyst on the niobium electrode with thin SiO_2 layer for the MIC diode. Figure 3.15 shows image of the whole MIC structure and SEM image of a vertical aligned multi-walled carbon nanotube (MWCNT). The advantages of MIC structure are that it is not only easy to acquire small junction area and control of the gap between metallic layers, but also good field emission effect due to high aspect ratio of a CNT ($\beta \approx 200\sim 2000$) as well as good conductivity.

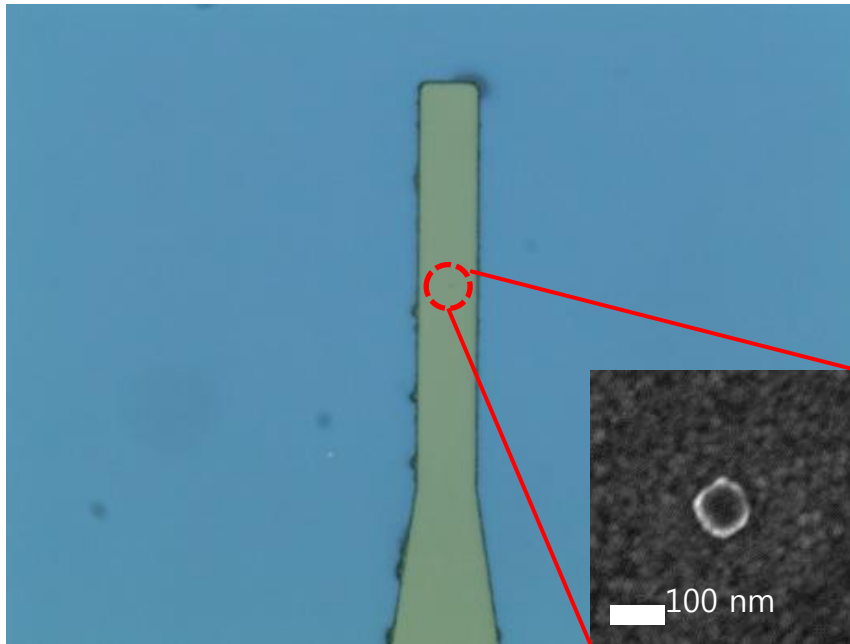


Figure 3.14: The photo image and SEM image after forming catalyst on the Nb bottom electrode with thin SiO₂ layer for the MIC diode

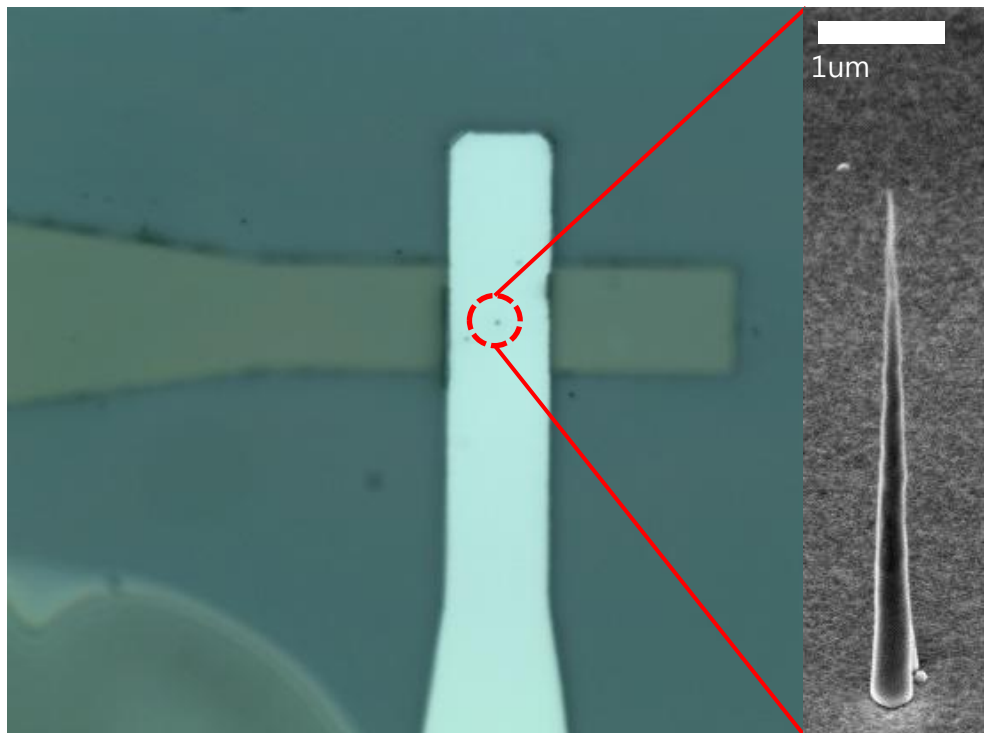


Figure 3.15: The photo image of the whole MIC structure and SEM image of a vertical aligned multi-walled carbon nanotube (MWCNT) using PECVD with C₂H₂/NH₃ gas flow, 600V of plasma intensity, 650 °C of temperature, and 10 minute of growth time on patterned Ni catalyst position

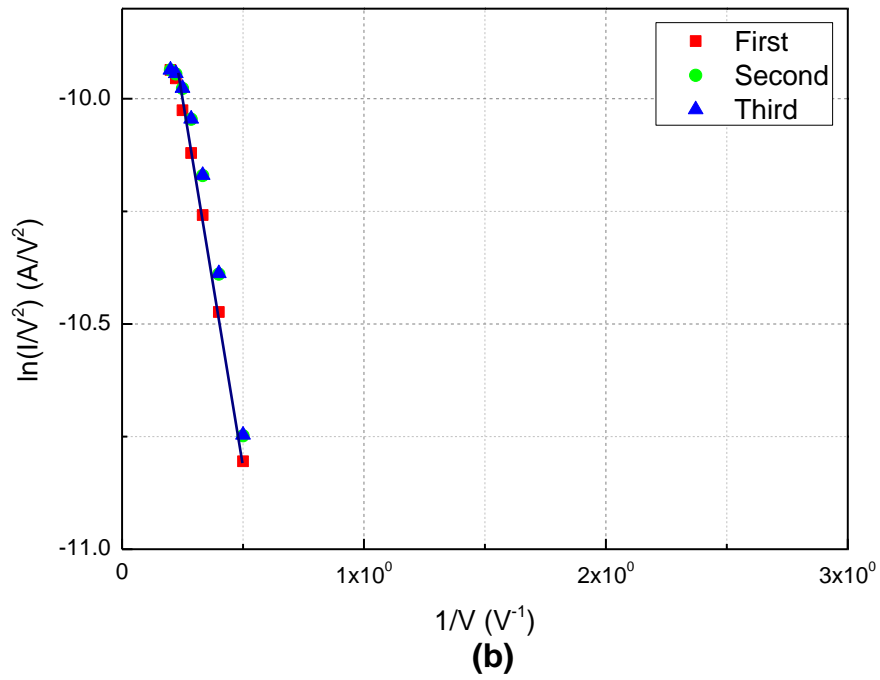
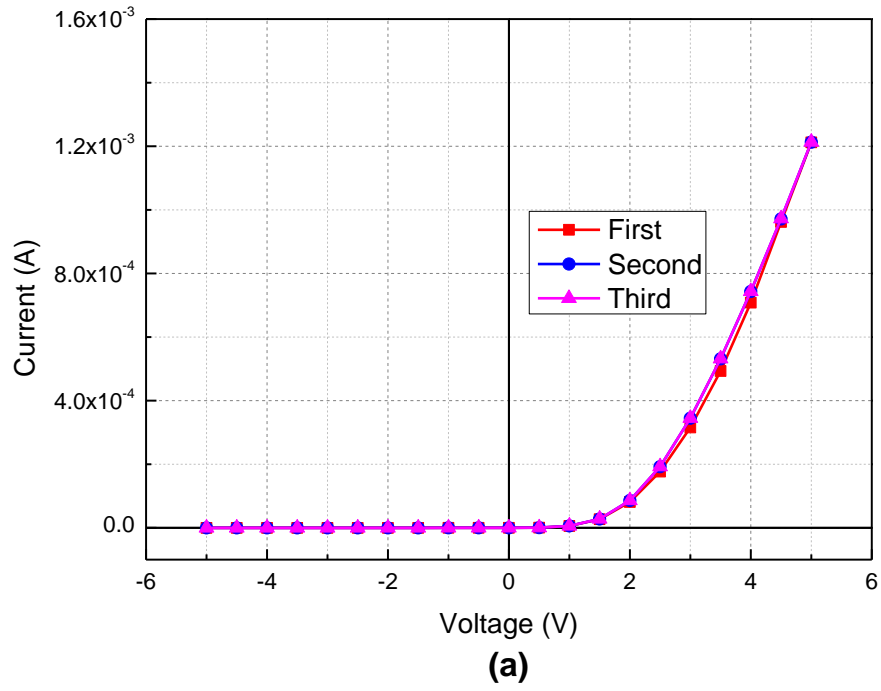


Figure 3.16: The electrical characteristics of MIC diode (a) I-V curve of Nb-SiO₂-MWCNT structure (b) the plot based on Fowler-Nordhiem tunneling model

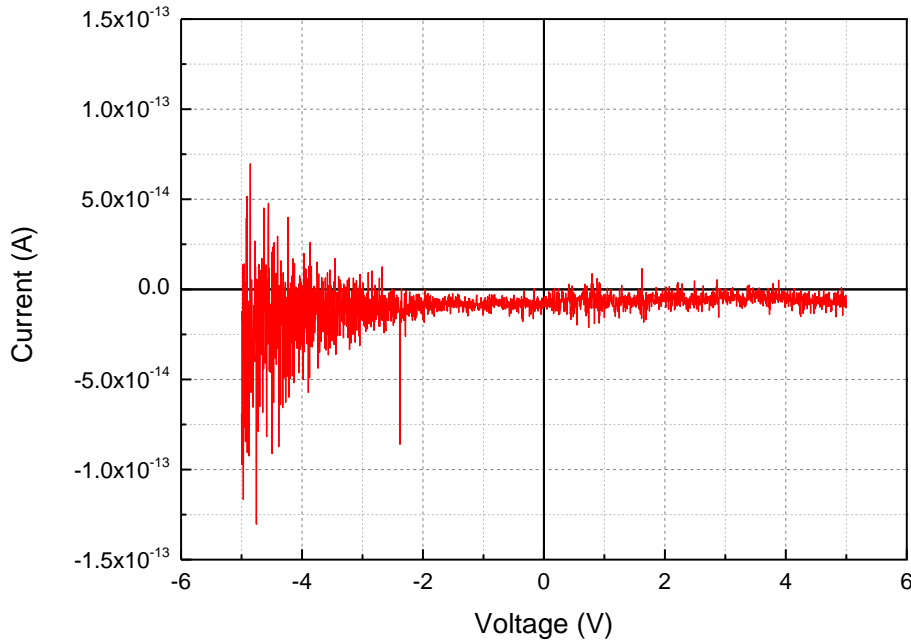


Figure 4.17: I-V characteristics of MIC structure without a CNT

Figure 3.16 shows the asymmetric I-V characteristics with low leakage current. This behavior is much better than the characteristics of lateral MIM structure. The much lower threshold voltage means that it can rectify much higher frequency. This straight line in the plot based on Fowler-Nordhiem tunneling model indicates that the current flow is mainly induced by the tunneling effect. To verify the pathway to flow current, the MIC structure without a CNT was fabricated and measured. Figure 3.17 shows I-V characteristics of MIC structure without a CNT. The current level is several fA so that we sure that the almost electrons pass through Nb-SiO₂-CNT pathway. Thus, the MIC structure is very suitable for diode behavior. However, the threshold turn-on voltage is as high as 1V, mainly depending on thickness of oxide layer. Even though the thickness of SiO₂ layer of the sample is about 40 nm as same as the lateral MIM structure, it has much higher current flow. We assume that the electrical properties of a CNT can induce much higher tunneling current.

If the thickness decreases, much lower threshold can be obtained. The MIC structure is easier control the thickness of oxide layer due to bottom-up structure, compared to lateral MIM structure. The estimated maximum cut-off frequency is 3.47 THz.

3.4 Rectification performance

Rectification performance from AC signal is much more practical result than I-V characteristics so that it should be studied three kinds of the MIM structures. I-V curves were measured under DC bias state; however, rectification is to convert AC signal to DC signal. The conversion efficiency and cut-off frequency can be studied under AC source state. Thus, these factors were measured by two channel oscilloscope, Tecktronix's TDS 2012C. The AC source was generated by wave form generator, Agilent's 33250A. Figure 3.18 is the measurement set-up for rectification performance. The four kinds of diodes, commercial Schottky, simple MIM ($\text{Al-AlO}_x\text{-Pt}$), lateral MIM, and MIC diode, were measured to compare the rectification performance each other. The measurement was performed with the frequency (60 Hz ~ 80 MHz) and voltage (-10 V ~ 10 V), due to the equipment limitation.

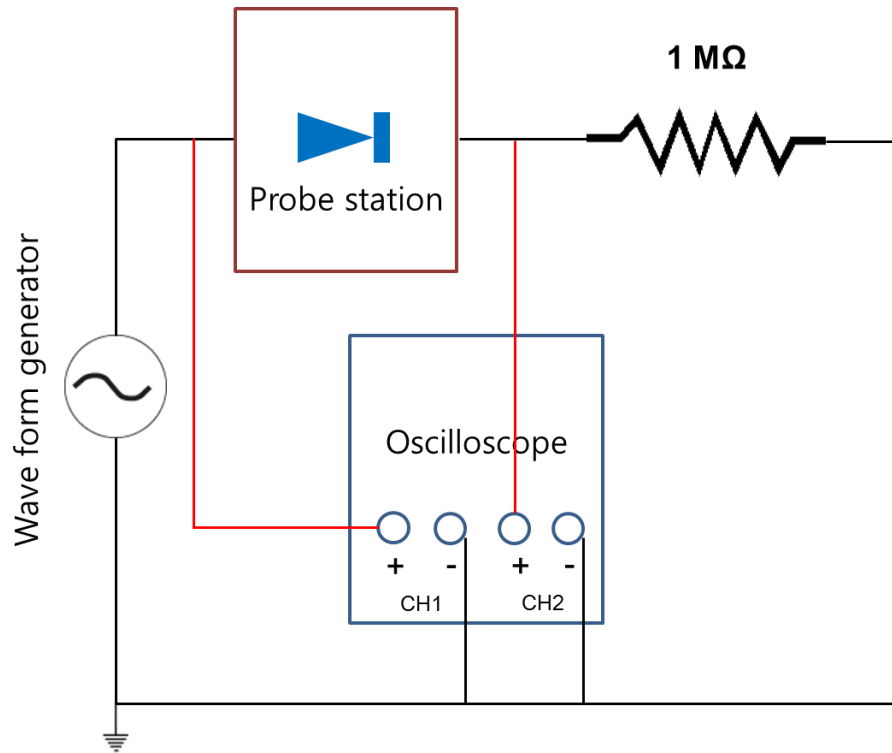


Figure 3.18: the measurement set-up for rectification performance

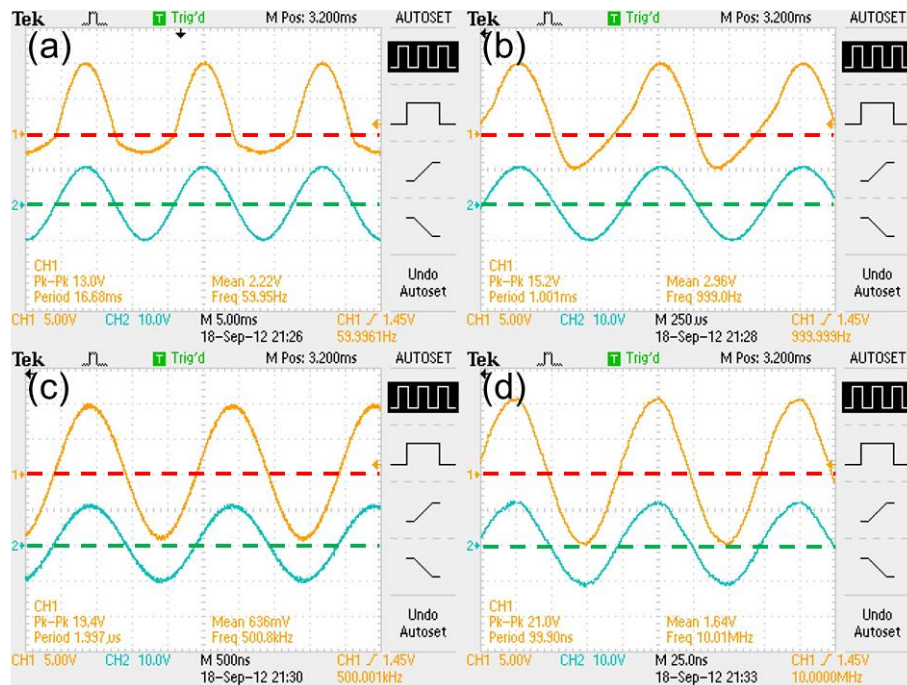


Figure 3.19: Rectification performance of Schottky barrier diode (a) 60 Hz (b) 1 kHz (c) 500 kHz (d) 10

MHz

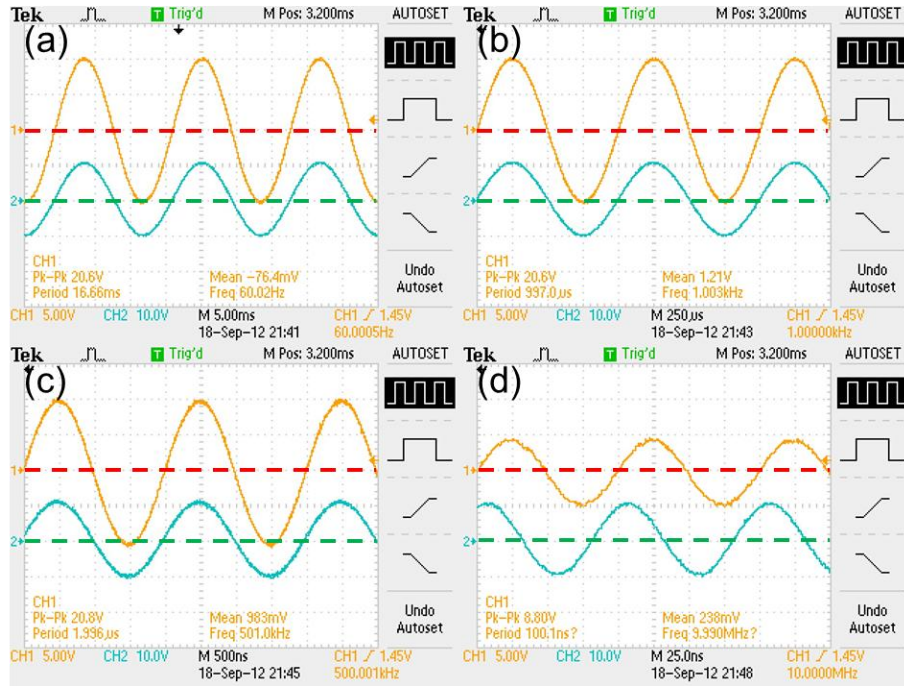


Figure 3.20: Rectification performance of simple MIM diode (a) 60 Hz (b) 1 kHz (c) 500 kHz (d) 10 MHz

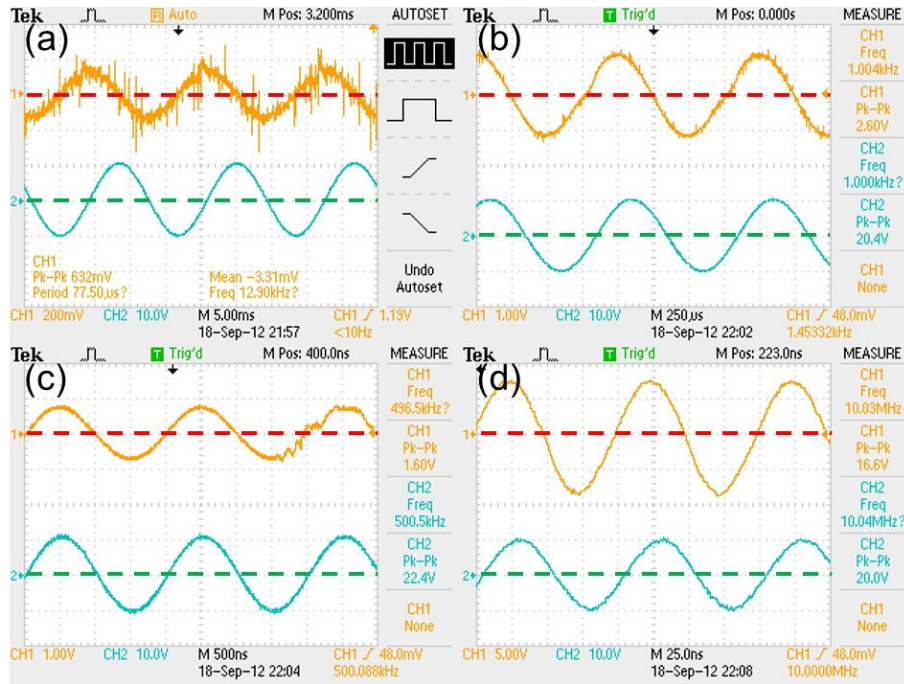


Figure 3.21: Rectification performance of lateral MIM diode (a) 60 Hz (b) 1 kHz (c) 500 kHz (d) 10 MHz

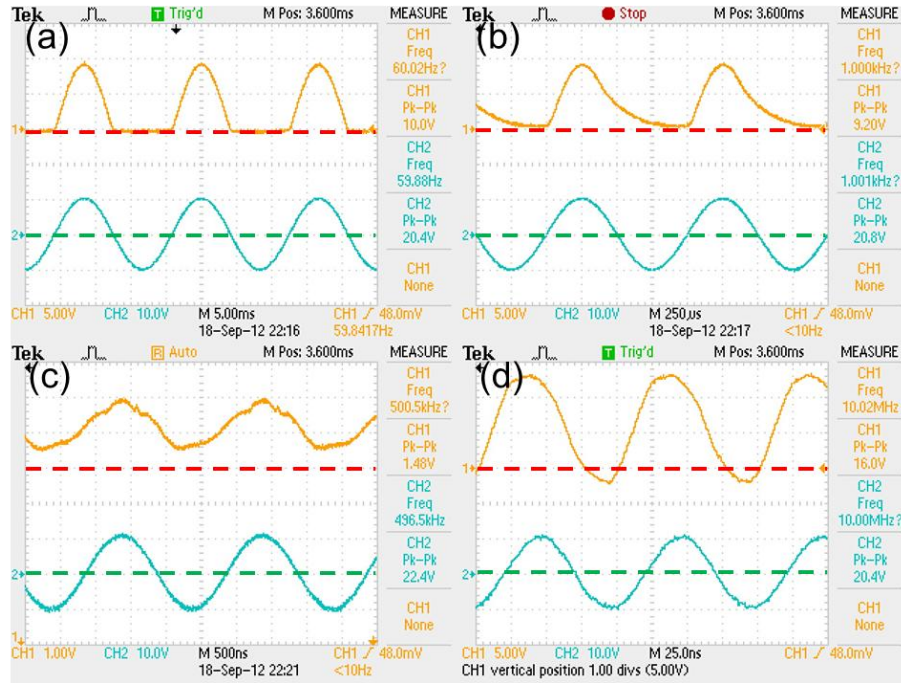


Figure 3.22: Rectification performance of MIC diode (a) 60 Hz (b) 1 kHz (c) 500 kHz (d) 10 MHz

Figure 3.19 ~ 22 show the rectification performance of Schottky, simple MIM (Al-AIO_x-Pt), lateral MIM, and MIC diode, in sequence. The upper line is an output signal and the bottom line is the input signal. The almost AC signal into the simple MIM diode passes without rectification. As mentioned previously, because it has symmetric I-V curve, its behavior is similar to resistance. In the graph of lateral MIM diode, it is also similar to the simple MIM diode, because the threshold voltage is over 20 V; thus, it cannot rectify below 20 V source. Although the rectification performance of Schottky barrier diode is good at 60 Hz, over 1 kHz too much the leakage current takes place. However, the MIC diode shows a perfect rectification performance without the leakage current at 60 Hz. From 60 Hz to 10 MHz, its rectification performance is quite a good. As increasing frequency, the output signal is changed. At 10 MHz, the few negative bias passes through the diode.

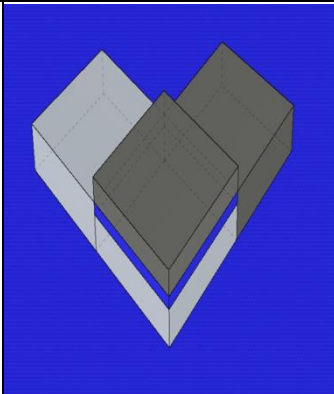
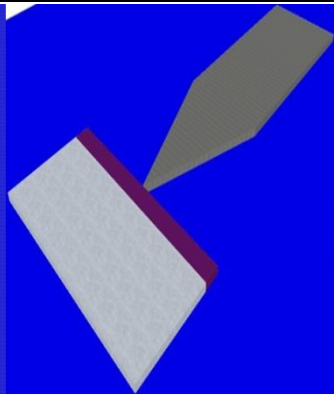
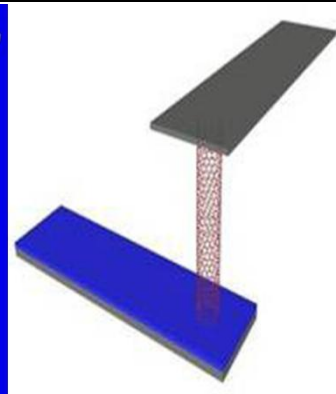
IV. CONCLUSION

The simple MIM, the lateral MIM, and the MIC diode have been fabricated and studied to rectify the high frequency wave to DC signal for various applications, such as communication, biology, energy harvesting, and so forth. Table 4.1 provides comparison with the three devices which have been fabricated.

The simple MIM diode has very low capacitance and resistance from thin native oxide layer as small as about 2 ~ 7 nm so that it can provide a good opportunity to operate at high frequency; however, its non-linearity is very poor. The lateral MIM diodes has very sharp tip to overcome the lack of non-linearity. Even though this asymmetric structure is better to get more non-linearity, its threshold voltage is quite high due to the gap as long as 41 nm between two electrodes. If gap as small as about 10 nm can be formed, this structure can be a good candidate of the high frequency MIM diode. It depends on fabrication technique, especially in E-Beam lithography step. In our case, the lateral MIM diode is hard to control the gap size so that we come up with novel structure, MIC diode. The performance of MIC diode is the best in both non-linearity and cut-off frequency compared to the simple and lateral MIM diode. Although in MIC diode case the oxide thickness is about 40 nm, the non-linearity, asymmetry, and cut-off frequency of the MIC diode is a better than the others due to FE effect from high aspect ratio of a CNT. If the thickness of the oxide layer decrease, higher performance is expected; however, too thin oxide layer can induce symmetric I-V characteristics so that the thickness of the oxide layer should be optimized. The three types of MIM diode are introduced to obtain high performance, especially for non-linearity and high cut-off frequency. The best model among three devices is MIC diode. This asymmetric structure is better to get non-linearity and using a CNT is one of the solutions to overcome

trade-off between resistance and capacitance. The structure effect is considered to be ideal high frequency diode. It shows a good rectifying performance up to 10 MHz in direct measurement mode and the estimated maximum cut-off frequency is 3.47 THz.

Table 4.1 Comparison with the simple MIM diode, lateral MIM diode, MIC diode

	Simple MIM diode	Lateral MIM diode	MIC diode
Schematic illustration			
Structure	Simple structure	Lateral point contact Structure (For field emission effect)	Vertical point contact Structure (For field emission effect)
Non-linearity	Poor	Good	Best
Asymmetric I-V characteristics	Poor	Good	Best
Tunneling	-	Good	Best
Resistance	Very small	Very high	Very small
Capacitance	Small	Small	Small
Cut-off Frequency	High	15.47 Hz	3.471 THz

References

- [1] http://en.wikipedia.org/wiki/P%E2%80%93n_junction
- [2] S. O. Kasap. (2006). *principle of electronic materials and devices 3rd edition*, mcgraw hill international edition, 876 pages
- [3] O. Acef, L. Hilico, M. Bahoura, F. Nez, and P. De Natale. (1994). “Comparison between MIM and Schottky diodes as harmonic mixers for visible lasers and microwave sources,” *Optics communications*, vol. 109, no. 5, pp. 428–434.
- [4] http://electriciantraining.tpub.com/14183/css/14183_137.htm
- [5] L. Esaki. (1958) “New Phenomenon in Narrow Germanium p-n Junctions,” *Phys. Rev.*, vol. 109, no. 2, pp. 603–604.
- [6] http://electriciantraining.tpub.com/14183/css/14183_142.htm
- [7] S. M. Sze and K. K. Ng. (1981 & 2006). *Physics of semiconductor devices*, Wiley-interscience, 815 pages
- [8] M. Heiblum, S. Wang, J. Whinnery, and T. Gustafson. (1978). “Characteristics of integrated MOM junctions at dc and at optical frequencies,” *Quantum Electronics, IEEE Journal of*, vol. 14, no. 3, pp. 159–169.
- [9] B. Berland. (2003). “Photovoltaic Technologies Beyond the Horizon: Optical Rectenna Solar Cell.”
- [10] Subramanian, Krishnan. (2004). “Design, fabrication and characterization of thin-film M-I-M diodes for rectenna array.” *Master. Thesis*, University of South Florida, USA, 84 pages
- [11] J. A. Bean. (2009). “Thermal Infrared Detection Using Antenna-Coupled-Metal-Oxide-Metal Diodes”, *Ph.D. Thesis*, University of Notre Dame, Indiana, USA, 147 pages.
- [12] E. W. Cowell III, N. Alimardani, C. C. Knutson, J. F. Conley Jr, D. A. Keszler, B. J. Gibbons, and J. F. Wager. (2011). “Advancing MIM electronics: Amorphous metal electrodes,” *Advanced Materials*, vol. 23, no. 1, pp. 74–78.

[13] X. Sun. (2006). “Designing efficient field emission into ZnO,” SPIE Newsroom, The International Society for Optical Engineering, s. 1C4.

[14] <http://en.wikipedia.org/wiki/Nantenna>

[15] P. Esfandiari, G. Bernstein, P. Fay, W. Porod, B. Rakos, A. Zarandy, B. Berland, L. Boloni, G. Boreman, B. Lail, and others. (2005). “Tunable antenna-coupled metal-oxide-metal (MOM) uncooled IR detector,” in Proc. of SPIE Vol, vol. 5783, p. 471.

[16] <http://en.wikipedia.org/wiki/Diode>

[17] J. E. Jang, S. N. Cha, Y. J. Choi, D. J. Kang, T. P. Butler, D. G. Hasko, J. E. Jung, J. M. Kim, and G. A. J. Amaratunga. (2008). “Nanoscale memory cell based on a nanoelectromechanical switched capacitor,” Nature Nanotechnology, vol. 3, no. 1, pp. 26–30.

[18] M. Koch. (2007). “Terahertz Frequency Detection and Identification of Materials and Objects.” Nato Science for Peace and Security Series—B: Physics and Biophysics, Springer Science and Business Media, Dordrecht, Netherlands, pp.325–338.

[19] S. Grover, O. Dmitriyeva, M. J. Estes, and G. Moddel. (2010). “Traveling-Wave Metal/Insulator/Metal Diodes for Improved Infrared Bandwidth and Efficiency of Antenna-Coupled Rectifiers,” IEEE Transactions on Nanotechnology, vol. 9, no. 6, pp. 716 –722.

[20] H. Kazemi, K. Shinohara, G. Nagy, W. Ha, B. Lail, E. Grossman, G. Zummo, W. R. Folks, J. Alda, and G. Boreman. (2007). “First THz and IR characterization of nanometer-scaled antenna-coupled InGaAs/InP Schottky-diode detectors for room temperature infrared imaging,” in Defense and Security Symposium, p. 65421J–65421J.

[21] I. Codreanu, F. J. Gonzalez, and G. D. Boreman. (2003). “Detection mechanisms in microstrip dipole antenna-coupled infrared detectors,” Infrared physics & technology, vol. 44, no. 3, pp. 155–163.

[22] Y. Cheng and O. Zhou. (2003). “Electron field emission from carbon nanotubes,” Comptes Rendus Physique, vol. 4, no. 9, pp. 1021–1033.

[23] B. J. Eliasson. (2001). “Metal-insulator-metal diodes for solar energy conversion,” University of Colorado.

- [24] P. Periasamy, J. D. Bergeson, P. A. Parilla, D. S. Ginley, and R. P. O'Hayre. (2010). "Metal-insulator-metal point-contact diodes as a rectifier for rectenna," in Photovoltaic Specialists Conference (PVSC), 2010 35th IEEE, pp. 002943–002945.
- [25] P. C. D. Hobbs, R. B. Laibowitz, and F. R. Libsch. (2005). "Ni- NiO- Ni tunnel junctions for terahertz and infrared detection," *Applied optics*, vol. 44, no. 32, pp. 6813–6822.
- [26] B. Berland, L. Simpson, G. Nuebel, T. Collins, and B. Lanning. (2003). "Optical rectenna for direct conversion of sunlight to electricity," *Physics Review*, pp. 323–324.
- [27] A. Sanchez, C. F. Davis, K. C. Liu, and A. Javan. (1978). "The MOM tunneling diode: Theoretical estimate of its performance at microwave and infrared frequencies," *Journal of Applied Physics*, vol. 49, no. 10, pp. 5270–5277.
- [28] J. G. Simmons. (1963). "Low-Voltage Current-Voltage Relationship of Tunnel Junctions," *Journal of Applied Physics*, vol. 34, no. 1, pp. 238–239.
- [29] J. G. Simmons. (1963). "Generalized formula for the electric tunnel effect between similar electrodes separated by a thin insulating film," *Journal of Applied Physics*, vol. 34, no. 6, pp. 1793–1803.
- [30] B. Twu and S. E. Schwarz. (1974). "Mechanism and properties of point-contact metal-insulator-metal diode detectors at $10.6\ \mu$," *Applied Physics Letters*, vol. 25, no. 10, pp. 595–598.

요 약 문

고주파를 이용한 다양한 응용을 위한 Metal-Insulator-Metal 다이오드

본 논문은 고속동작을 위한 MIM 다이오드의 전기적 성질을 구조적 효과에 의해 향상시키는 것에 초점을 두고 있다. 최근에 고속 컴퓨터, 광학, 통신분야 등 많은 분야에서 고속 동작의 소자들이 요구되어 지고 있다. 이로인해 요구되어 지는 주파수 범위는 거의 terahertz 까지 높아졌다. 따라서 이런 동작 주파수 범위를 갖는 고속 소자들이 필요하다. 그 중 각 분야에 꼭 필요로하는 소자 중에 하나가 정류소자인 다이오드이다. Schottky 다이오드는 일반적으로 AC 신호를 DC 신호로 바꿔주는 정류를 고주파에서도 가능하다. 그러나 이 소자의 작동 주파수는 몇 테라헤르츠까지로 제한 되어있다. MIM 다이오드는 이런 제한을 넘어서 더 빠른 고속 동작이 가능한 소자이다. 이 소자로 인해 다양한 테라헤르츠 응용이 가능하다.

하지만 더 높은 주파수에서의 동작을 위해서 MIM 다이오드도 개선 해야 할 요소가 있다. 고속 동작의 다이오드는 전류-전압 그래프가 비선형성과 비대칭성을 가져야 하고 시정수가 짧아야 한다. 하지만 MIM 다이오드는 짧은 시정수를 위해 절연막을 얇게 만들고 접촉면적을 줄였다. 하지만 이로 인해 비선형성과 비대칭성이 감소 되었다. 따라서 짧은 시정수와 함께 구조적인 비대칭성으로 비선형성을 향상시키는 것이 이 논문의 목적이다. 그래서 simple MIM 다이오드, 수평구조의 MIM 다이오드, 그리고 MIC (metal-insulator-carbon nanotube) 다이오드를 연구하였다. 구조적인 효과와 물질 적인 효과를 고려하여서 제작한 수평구조의 MIM 다이오드, MIC 다이오드는 비선형성과 비대칭성을 가진다. 그리고 또한 MIC 다이오드의 경우에는 10 MHz 까지는 아주 좋은 정류 성질을 보여주고, 추정하고 있는 cut-off 주파수는 약 3.47 THz 이다.

핵심어: 테라헤르츠, MIM 다이오드, 고속 동작

Acknowledgement

It is my great pleasure to thank everyone who has supported to make this work be possible. First and foremost, I am sincerely thankful to my advisor, Prof. Jae Eun Jang, for his guidance and unstinted support throughout my research. He has not only given many knowledge and novel ideas, but also taken time to patiently discuss every detail of the work. He has provided me with every opportunity to be successful and has supported me in every manner.

I would also like to thank Prof. YounGu Lee and Prof. Min-Soo Kim as committee members. They have given me sincere interest and advisor. I would like to thank a member of CCRF of DGIST: Hwan Soo Jang and a member of KANC: Sang Hyun Jung for his theoretical and fabrication expertise especially maskless photolithography and E-Beam lithography, respectively. I would like to thank Faculty members of department of Information and Communication Engineering of DGIST: Prof. Wook Hyoun Kwon, Prof. Sang Hyuk Son, Prof. Ji-Woong Choi, Prof. Taejoon Park, and Prof. Kyung-Joon Park; they have usually provided many opportunities to enhance the academic techniques and skills. My colleagues in our department have given me the encouragement: especially to Hyerin Kim, Jaehan Im, Seunguk Kim, Yeri Jung, and Jonggu Kang.

Finally, I would like to thank beloved grandmother, father, mother, younger brother, relatives, and many close friends and dedicate this thesis to grandfather in heaven.